

## RESEARCH ARTICLE

10.1029/2019JC015984

## Special Section:

Coastal hydrology and oceanography

This article is a companion to Wang et al., (2020), <https://doi.org/10.1029/2019JG005569>.

## Key Points:

- We employ a Lagrangian observation of diverse productivity measurements in the California Current
- Temporally highly resolved productivity, based on optical and mass spectrometric methods, was comparable with traditional in situ 24-h assays
- We suggest that temporally resolved production methods be employed regularly to enhance understanding of physically complex ecosystems

## Supporting Information:

- Supporting Information S1

## Correspondence to:

S. A. Kranz,  
skranz@fsu.edu

## Citation:


Kranz, S. A., Wang, S., Kelly, T. B., Stukel, M. R., Goericke, R., Landry, M. R., & Cassar, N. (2020). Lagrangian studies of marine production: A multimethod assessment of productivity relationships in the California Current Ecosystem upwelling region. *Journal of Geophysical Research: Oceans*, 125, e2019JC015984. <https://doi.org/10.1029/2019JC015984>

Received 3 JAN 2020

Accepted 28 MAR 2020

Accepted article online 16 APR 2020

# Lagrangian Studies of Marine Production: A Multimethod Assessment of Productivity Relationships in the California Current Ecosystem Upwelling Region

Sven A. Kranz<sup>1</sup> , Seaver Wang<sup>2</sup> , Thomas B. Kelly<sup>1</sup> , Michael R. Stukel<sup>1,3</sup> , Ralf Goericke<sup>4</sup>, Michael R. Landry<sup>4</sup> , and Nicolas Cassar<sup>2</sup> 

<sup>1</sup>Department of Earth, Ocean and Atmospheric Science, Florida State University, Tallahassee, FL, USA, <sup>2</sup>Division of Earth and Ocean Sciences, Duke University, Durham, NC, USA, <sup>3</sup>Center for Ocean-Atmospheric Prediction Studies, Florida State University, Tallahassee, FL, USA, <sup>4</sup>Integrative Oceanography Division, Scripps Institution of Oceanography, La Jolla, CA, USA

**Abstract** A multimethod process-oriented investigation of diverse productivity measures in the California Current Ecosystem (CCE) Long-Term Ecological Research study region, a complex physical environment, is presented. Seven multiday deployments covering a transition region from high to low productivity were conducted over two field expeditions (spring 2016 and summer 2017). Employing a Lagrangian study design, water parcels were followed over several days, comparing 24-h in situ measurements (<sup>14</sup>C and <sup>15</sup>NO<sub>3</sub>-uptake, dilution estimates of phytoplankton growth, and microzooplankton grazing) with high-resolution productivity measurements by fast repetition rate fluorometry (FRRF) and equilibrium inlet mass spectrometry (EIMS), and integrated carbon export measurements using sediment traps. Results show the importance of accounting for temporal and fine spatial scale variability when estimating ecosystem production. FRRF and EIMS measurements resolved diel patterns in gross primary and net community production. Diel productivity changes agreed well with comparably more traditional measurements. While differences in productivity metrics calculated over different time intervals were considerable, as those methods rely on different base assumptions, the data can be used to explain ecosystem processes which would otherwise have gone unnoticed. The processes resolved from this method comparison further understanding of temporal and spatial coupling and decoupling of surface productivity and potential carbon burial in a gradient from coastal to offshore ecosystems.

**Plain Language Summary** The California Current Ecosystem (CCE) is a site of coastal upwelling and is among the most productive ecosystems in the world oceans, supporting fisheries of much of the western United States, while playing a vital role in the economy of coastal communities. Accurately assessing marine productivity in such regions is important for understanding the flux of carbon through the food web and the ocean's ability to sequester carbon dioxide. Productivity assessments are, however, often based on different methodologies relying on distinct cellular or ecosystem assumptions. Each individual method can thus be misleading if its assumptions are not met, while any single method is likely to fall short in terms of explaining ecosystem dynamics. Here, we present a multimethod process-oriented investigation of diverse productivity methods in the CCE Long-Term Ecological Research study region. Traditional 24-h in situ incubation methods were compared with high temporal resolution measurements using advanced optical and mass spectrometric methods. The productivity rates and ecosystem processes resolved presented here can help to further our understanding of the linkages between photosynthesis and respiration or carbon production and sequestration. This approach can also help to improve productivity assessments in complex ecosystems and to resolve the timescales of these processes.

## 1. Introduction

Upwelling plays a key role in driving marine primary production along the eastern continental margins of the world's oceans, making these ecosystems some of the most productive regions in the world (Chavez & Messie, 2009; Dugdale, 1972; Dunne et al., 2007; Kudela et al., 2008; Longhurst et al., 1995; Muller-Karger et al., 2005). Upwelled water rich in inorganic nutrients support intense phytoplankton blooms, typically

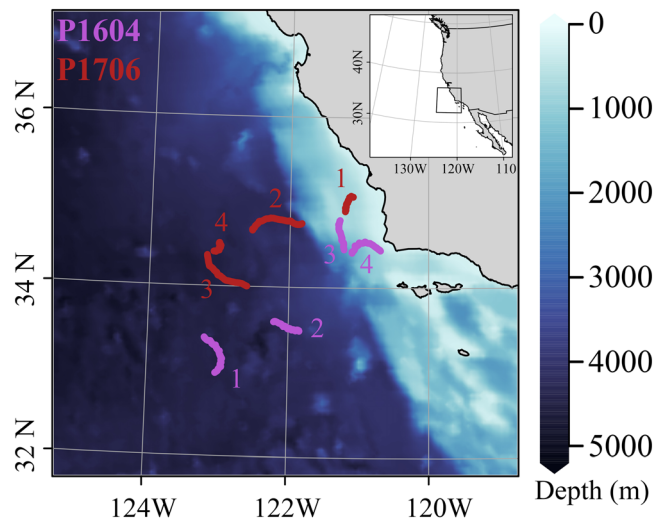


**Figure 1.** Map of Lagrangian study sites for cruises P1604 (purple) and P1706 (red). P1604 started in the west offshore and continues inshore. P1706 started in the east and continues further offshore. Colors indicate bathymetry.

dominated by large diatoms that efficiently transfer newly produced biomass to higher trophic levels and into the mesopelagic via sinking (Kumar et al., 1995; Michaels & Silver, 1988; Stock & Dunne, 2010; Thunell et al., 2007). Lateral transport also provides a significant flux of upwelled nutrients and coastal planktonic communities to the offshore domain (Nagai et al., 2015; Plattner et al., 2005), resulting in complicated spatial and temporal connectivity between physical forcing, in situ community composition and regional biogeochemistry.

While remote sensing techniques can reasonably quantify phytoplankton standing stocks (O'Reilly et al., 1998; Saba et al., 2011), primary production (Behrenfeld & Falkowski, 1997; Kahru et al., 2015), and even community composition (Pan et al., 2011; Uitz et al., 2015), over broad temporal and spatial scales, fine-scale and subsurface features remain challenging to resolve from satellites. Shipboard incubation techniques allow more accurate measurements throughout the photic zone, but cannot resolve highly spatially variable patterns in heterogeneous regions. In addition, shipboard methods with different assumptions, caveats, and spatiotemporal integration scales can be challenging to compare among cruises and regions. Consequently, multimethod approaches for assessing productivity have proven useful for understanding the nuances of processes that shape production responses to varying environmental conditions

and their relationships (e.g., Hamme et al., 2012; Quay et al., 2010; Robinson et al., 2009; Teeter et al., 2018).

Here, we take such a multimethod approach to reveal commonalities and complications among several ecosystem production techniques applied to heterogeneous environmental settings in the California Current Ecosystem (CCE) from coastal upwelling to the oligotrophic open ocean. We especially want to emphasize that novel productivity assessment techniques can reveal high temporal and spatial resolution of marine productivity which can in turn prove useful in characterizing ecosystem productivity patterns. In the following section, we first touch briefly on the various definitions and methods for assessing primary productivity and their issues. We then describe process-oriented investigations on two field expeditions (spring 2016 and summer 2017; Figure 1) in the CCE Long-Term Ecological Research (LTER) study region off of southern California on which we compared traditional in situ measurements ( $^{14}\text{C}$ ,  $^{15}\text{NO}_3^-$ , dilution-based growth rates, and sediment traps) for assessing net primary production (NPP), new production (NP), and export production to high-resolution production measurements of net carbon production (NCP),  $\text{O}_2$ :Ar-based gross primary production (GPP), and fast repetition rate fluorometry (FRRF)-based photophysiological measurements of GPP.

Two novel aspects of the study are highlighted. First, we utilized a Lagrangian approach, tracking water parcels for several days, which allowed us to follow the evolution of production processes during advective transport and to measure some aspects of diel variability. Second, we field tested and compared results for a new approach, described in detail in a companion paper (Wang et al., 2020), that uses  $\text{O}_2$ /Ar to resolve temporal and spatial patterns of NCP in a highly dynamic region. To our knowledge, this study comprises the first in-depth analysis of so many different production assessments in a highly dynamic coastal setting. While some differences are noted, as expected from the different processes measured, results from temporally resolved production approaches are surprisingly consistent with traditional production measurements, indicating that such approaches could provide important new insights into the production dynamics of physically complex systems.

## 2. Overview of Production Definitions and Measurement Approaches

The many different techniques for assessing ocean production can be reasonably grouped in a few broadly defined measurement categories. GPP is the rate of organic carbon production by autotrophs. NPP refers to GPP minus the respiration performed by the autotrophs themselves. NPP thus accounts for both growth and metabolic loss processes that lead to phytoplankton biomass production. NP refers to the portion of phytoplankton production based on the uptake of “new” nitrogen (N) that enters the euphotic zone from

external sources. NP sources include upwelled  $\text{NO}_3^-$ , believed to be the dominant source of new nitrogen in the CCE, as well as nitrogen delivered by atmospheric deposition, riverine input, or nitrogen fixation. Export production measures the rate of carbon exported out of the euphotic zone where primary production occurs, which is generally defined as the depth of penetration of 1% or 0.1% surface irradiance. Net community production (NCP), sometimes also called net ecosystem production, is defined as GPP minus the respiration of all organisms in the ecosystem. As most production is eventually respired at the community level, NCP rates need to be constrained by depth or time boundaries. When integrated over appropriate spatial and temporal scales and converted to common units, NCP, NP, and export production should be in balance, representing the total amount of carbon or nitrogen that can be exported from the euphotic zone by the biological carbon pump without depleting biomass (Eppley & Peterson, 1979).

One of the most common methods for estimating primary production is the incorporation of  $^{14}\text{C}$ -labeled bicarbonate into particulate organic carbon (Steemann Nielsen, 1952). Although this highly sensitive method has been a standard for aquatic production studies for decades, interpretation is still highly debated (Marra, 2009; Peterson, 1980). Measurements conducted over a relatively short time approximate GPP, but longer incubations have increasing losses to respiration. Experiments conducted over the full 24-h photocycle are thought to approach NPP, but should be underestimates because the respiratory losses include contributions from heterotrophs that have consumed labeled C, in addition to respiration from autotrophs. Interpretations are further complicated by starting incubations at different times of day, requiring different weighting for uptake and respiration. Additionally, production can be significantly underestimated when incorporation of  $^{14}\text{C}$  into dissolved organic carbon (DOC) is unmeasured (Laws et al., 2000; Mykkestad, 2000; Teira et al., 2001). NPP can also be assessed by the seawater dilution method, where serial dilution is used to decouple growth and grazing processes, allowing separate instantaneous rate estimates for phytoplankton growth and microzooplankton grazing (Landry & Hassett, 1982). When carbon-based biomass estimates for phytoplankton is combined with dilution-based daily rates, the calculated NPP result is the daily net carbon biomass produced by phytoplankton absent losses that are a consequence of grazing (Barron et al., 2014; Landry et al., 2000).

The uptake and incorporation of  $^{15}\text{NO}_3^-$  into phytoplankton cells can also be used to estimate phytoplankton production derived from that nitrogen source (Dugdale & Goering, 1967). The  $^{15}\text{N-NO}_3^-$  method is thought to reduce the impact of internal elemental turnover, a process much enhanced in the cellular carbon pool compared with cellular nitrogen. The measurement is based on the enrichment of  $^{15}\text{N}$  in cellular particulate organic nitrogen (PON) over the incubation period and is defined as NP, under the assumption that nitrate is not regenerated from ammonium in the euphotic zone. This method can, however, be impacted by processes such as ammonification or nitrification in surface waters (Yool et al., 2007), which lead to underestimates or overestimates of NP. In addition, luxury  $\text{NO}_3^-$  uptake (Painter et al., 2007) and release of previously fixed  $^{15}\text{N}$  as DON can also affect results of the  $^{15}\text{N}$  method (Bronk et al., 1994; Collos, 1998).

NCP, the balance between photosynthesis and community respiration, can be measured from the oxygen budget of the ocean mixed layer. Because of the similar physical properties of  $\text{O}_2$  and Ar, NCP measurements based on the  $\text{O}_2/\text{Ar}$  method are mostly immune to mixed-layer physical effects (e.g., solubility, gas exchange) on  $\text{O}_2$  budgets over timescales of days to weeks. However, coastal upwelling systems complicate the assumptions for this method (Teeter et al., 2018) since such coastal water parcels exhibit a larger magnitude of short-term variations in productivity and are subject to strong vertical fluxes that can alter surface  $\text{O}_2/\text{Ar}$ . Nonetheless, recent work has shown that NCP can be applied on shorter timescales (Hamme et al., 2012) if the measurements are conducted in a Lagrangian reference framework. Shortcomings of and improvements on this method, which is used in our CCE method comparison, are discussed in detail in a companion paper by Wang et al. (2020).

Short-term measurements by the  $\text{O}_2/\text{Ar}$  method can also be used to estimate GPP if done in the same Lagrangian-tracked water mass during the day (production + respiration) and night (respiration) and assuming that nighttime respiration rate applies to the day. GPP is more rigorously determined using isotopically labeled water ( $\text{H}_2^{18}\text{O}$ ) (Goldman et al., 2015) or oxygen ( $^{18}\text{O}_2$ ) (Kranz et al., 2010) or from the natural isotopic composition of oxygen by the  $^{17}\Delta\text{O}_2$  triple  $\text{O}_2$  isotope method (Luz & Barkan, 2005). However, these methods do not allow for high-resolution spatiotemporal sampling and were not used here. Alternatively, the conversion of sunlight into a biological redox potential in phytoplankton (i.e., electron generation at

photosystem II; PSII) can be assessed indirectly by variable fluorometry to provide another noninvasive PSII photochemical approach for estimating GPP at fine spatiotemporal scales. Using the single turnover method (STM) (Falkowski & Kolber, 1993; Kolber & Falkowski, 1993; Moore et al., 2006; Oxborough et al., 2012; Suggett et al., 2001), cellular energy allocation between photochemical (energy generation and fixation of inorganic nutrients) and nonphotochemical (energy dissipation if excitation exceeds photochemical quenching) processes can be quantified. However, the interpretation of the fluorescence signal is affected by environmental conditions such as nutrient limitation, signal quenching under high-light intensities, as well as other methodological sensitivities. Recent studies have recommended multiple improvements to reduce uncertainties of the STM method (Boatman et al., 2019; Oxborough et al., 2012; Schuback & Tortell, 2019), some of which we have applied in the present study. Most notably, however, O<sub>2</sub>:Ar-based NCP and GPP and variable fluorescence-based GPP approaches are incubation-independent production measurements free from “bottle effects” and amenable to flow-through applications that enable high spatiotemporal resolution sampling.

### 3. Material and Methods

#### 3.1. Cruise Background

Production measurements were made during quasi-Lagrangian experiments conducted on two Process cruises of the CCE LTER Program (Figure 1). The first cruise (RAPID CCE-LTER cruise P1604, 19 April to 12 May 2016, *R/V Sikuliaq*) investigated ecosystem responses during the 2015–2016 El Niño (Jacox et al., 2016) and had a wide geographic focus ranging from coastal upwelling to oligotrophic offshore conditions (Morrow et al., 2018; Nickels & Ohman, 2018). The second cruise (P1706, 1 June to 2 July 2017, *R/V Roger Revelle*) followed community and biogeochemical changes along a mesoscale filament transporting coastal waters to the offshore domain. Experiments were thus conducted in a gradient ranging from newly upwelled water to aged waters with a declining phytoplankton bloom. During both cruises, three to four quasi-Lagrangian experiments (hereafter “cycles”) were conducted, yielding seven total cycles. Cycles averaged ~3.5 days during which the cruise track followed a satellite-tracked Lagrangian drifter (Figure 1). Deployment areas were first surveyed with a Moving Vessel Profiler (MVP) (Ohman et al., 2012) to ensure that they represented a cohesive water parcel free of strong frontal gradients. The cycle was then initiated by deploying a sediment trap array followed by an array used for in situ incubations (Landry et al., 2012; Stukel et al., 2013). Both arrays had a 3 × 1 m holey sock drogue centered at 15-m depth in the surface mixed layer and followed similar drift paths during the cycles.

#### 3.2. Chlorophyll-*a* and Inorganic Nutrients

During each day of a cycle, samples for chlorophyll and nutrients were taken with CTD Niskin bottles at eight depths spanning the photic zone. Chlorophyll-*a* was extracted following Strickland and Parsons (1972). A more detailed description of sample analysis can be found in the Supporting Information. Nutrient samples were filtered using a 0.1- $\mu$ m Acropak filter prior to freezing for shore-based analysis. Dissolved inorganic nutrients (nitrate, nitrite, silicate, phosphate, and ammonium) were analyzed using an automated flow injection autoanalyzer on a Lachat Instruments QuikChem 8000 (Gordon et al., 1992). The precision of these measurements was  $\pm 5\%$ , and the detection levels for nitrate + nitrite, nitrite, ammonium, phosphate, and silicate were 0.2, 0.1, 0.1, 0.1, and 1.0  $\mu$ M, respectively.

#### 3.3. Bottle Incubations: NPP<sub>14C</sub> and <sup>15</sup>NO<sub>3</sub><sup>−</sup> NP

<sup>14</sup>C net primary production (NPP<sub>14C</sub>) and <sup>15</sup>NO<sub>3</sub><sup>−</sup> based NP were quantified from in situ incubations for each day of the cycles at six depths spanning the euphotic zone. Niskin bottle samples were gently transferred to polycarbonate incubation bottles (triplicate 250-ml bottles plus a dark bottle for NPP<sub>14C</sub> and a single 1-L bottle for NP) using silicon tubing. Samples were then spiked with H<sup>14</sup>CO<sub>3</sub><sup>−</sup> (NPP<sub>14C</sub>) or K<sup>15</sup>NO<sub>3</sub><sup>−</sup> (NP) and incubated for 24 h in mesh bags hung below the drift array. Incubations were started and terminated at ~04:00 local time. NPP<sub>14C</sub> samples were then filtered onto GF/F filters, acidified for 24 h (0.5 ml of 10% biological grade HCl), placed in scintillation cocktail, and subsequently counted using a liquid scintillation counter (details in Morrow et al., 2018). NP samples were filtered onto GF/F filters and frozen at sea. On land, they were acidified (fumed concentrated [37%] HCl), dried, and analyzed by isotope ratio mass spectrometry at the UC Davis Analytical Facility. Nitrate uptake was calculated following Dugdale and

Wilkerson (1986) with a slight modification similar to  $\rho_{is}$  in Kanda et al. (2003) when the nitrate spike was >10% of ambient nitrate (Stukel et al., 2016). On the P1706 cruise,  $NPP_{14C}$  samples were lost and  $NPP_{14C}$  was estimated using an algorithm fitted to CCE  $NPP_{14C}$  data, as described below.

### 3.4. Net Production Estimates Based on Chlorophyll, Light, and Nutrients

For the P1706 cruise, we estimated NPP rates from ambient light, nutrients, and Chl *a* as described by Stukel, Goericke, and Landry (2019). The initial algorithm was developed using irradiance to predict Chl *a*-specific production (Morrow et al., 2018) and then adapted for general use in the CCE. The algorithm was parameterized from data collected on seven previous CCE-LTER process cruises for which  $^{14}C$ -PP data were available. P1706 NPP was subsequently calculated as

$$\frac{NPP}{Chl} = V_{0m} \cdot \left(1 - e^{(-\alpha \cdot PAR/V_{0m})}\right) \cdot \frac{NH_4}{NH_4 + K_S}, \quad (1)$$

where  $NPP/Chl$  is the chlorophyll-specific primary production in units of  $mg\ C\ d^{-1}\ (mg\ Chl)^{-1}$ ; PAR is average daily photosynthetically active radiation (units of  $\mu mol\ photons\ m^{-2}\ s^{-1}$ ) within the mixed layer;  $(1 - \exp(-\alpha \cdot PAR/V_{0m}))$  describes the light saturation and inhibition term with  $V_{0m} = 66.5\ mg\ C\ d^{-1}\ (mg\ Chl)^{-1}$  and  $\alpha = 1.5$ ; and  $\frac{NH_4}{NH_4 + K_S}$  describes the ammonium limitation kinetics with  $K_S = 0.025\ \mu mol\ L^{-1}$ . Uncertainties in the algorithm were propagated through all subsequent equations following Stukel, Goericke, and Landry (2019). When averaged over the duration of a cycle, propagated errors in mixed layer NPP were  $\pm 30$ –40% at the 95% confidence limit.

### 3.5. Net Phytoplankton Production From Dilution Experiments ( $NPP_{G;G}$ )

To calculate phytoplankton intrinsic growth rates and microzooplankton grazing rates, dilution experiments were prepared following the two-treatment dilution approach (Landry et al., 2008; Landry et al., 2011b; Stukel et al., 2012). Each experiment consisted of water collected at six depths spanning the euphotic zone (i.e., “array depths”) in predawn CTD casts (02:00 local). At each depth, two 2.7-L polycarbonate bottles were filled with either unfiltered seawater (i.e., 100% whole seawater) or a mixture of 33% whole seawater and 67% 0.1- $\mu m$  filtered seawater. Samples were incubated in situ on the drifter array for 24 h along with the  $NPP_{14C}$  and NP experiments. Net growth rates in each bottle were determined from changes in fluorometrically measured Chl *a* and used to quantify gross growth rates ( $\mu$ ) and mortality due to protistan grazing ( $m$ ). Carbon to Chl *a* ratios (C:Chl) were determined using the approach of Li et al. (2010), based on microscopy-derived estimates of phytoplankton biomass in the CCE region. C:Chl was multiplied by Chl to determine initial carbon biomass ( $B_0$ ), and phytoplankton production was calculated as  $NPP_{G;G} = \mu B_0 e^{\mu - m} / (\mu - m)$ , following Landry et al. (2016).

### 3.6. Net and Gross Community Production From $O_2/Ar$ Measurements (NCP; $GPP_{O_2/Ar}$ )

Continuous samples of dissolved  $O_2/Ar$  were taken from the ship's underway seawater system.  $O_2/Ar$  gas ratios were measured with a Pfeiffer QMC 200 mass spectrometer equipped with an equilibration inlet (equilibrium inlet mass spectrometry [EIMS]) (Cassar et al., 2009). Temperature and oxygen concentrations were measured using Aandera temperature sensors (model 3835) and oxygen optodes. The signal was filtered to within an 8-km distance between the ship and the drifter (e.g., removing values during plankton net tows when the ship was far from the drifter location), and calibration and maintenance times were also removed. Net rates of community production (NCP) from  $O_2/Ar$  measurements reflect oxygen production by photoautotrophs, respiration by phototrophs and heterotrophs, and corrections for physical gas exchange processes. NCP rates are calculated for the mixed-layer depth (MLD) assuming no advective fluxes of  $O_2/Ar$  from neighboring water parcels and represent processes occurring over the residence time of  $O_2$  assuming a steady state system:

$$NCP_{prior} = k \cdot \Delta(O_2/Ar)[O_2]_{sol}\rho. \quad (2)$$

$NCP_{prior}$  estimates the time-averaged NCP based on wind speed history, MLD, and the observed biological oxygen signal, where  $k$  is the time-weighted piston velocity (see Reuer et al., 2007) incorporating the wind speed history and MLD.  $[O_2]_{sol}$  is the mixed layer oxygen solubility, and  $\rho$  is the average density of the mixed layer.  $\Delta(O_2/Ar)$  is the biological oxygen signal defined by  $\Delta(O_2/Ar) = \frac{(O_2/Ar)}{(O_2/Ar)_{atm}} - 1$ . Due to our Lagrangian

study design, we were able to measure short-term changes in mixed layer  $\Delta(O_2/Ar)$  in real time (“instantaneous changes”) and thereby estimate NCP over shorter timescales than the residence time of mixed layer  $O_2$  (see Hamme et al., 2012; Teeter et al., 2018; Wang et al., 2020).

$$NCP_{inst} = z \frac{\Delta(\Delta(O_2/Ar))}{\Delta t} [O_2]_{sol} \rho + \bar{k}(O_2/Ar)[O_2]_{sol} \rho, \quad (3)$$

where  $z$  denotes MLD and  $\bar{k}$  represents the instantaneous gas exchange coefficient averaged over the preceding hour (i.e.,  $\Delta t$ ). Using community respiration measured during the night,  $NCP_{(inst,night)}$  and assuming similar day and night respiration, GPP can be estimated as

$$GPP_{NCP} = NCP_{inst,day} - NCP_{inst,night}. \quad (4)$$

### 3.7. Estimating Mixed-Layer GPP Using FRRF

In addition to the  $O_2/Ar$  method, we also estimated GPP independently on the P1706 cruise based on the photophysiology of the mixed-layer phytoplankton community measured by FRRF. Shipboard measurements were made using a bench-top FastAct 2 + Fast TRAKA instrument (Chelsea, UK) plumbed into the ship's running seawater system. Photosynthesis versus irradiance ( $P$  vs.  $E$ ) curves were run continuously on a ~45-min sampling interval. Using a modified version of the absorbance algorithm following Oxborough et al. (2012), volume-based productivity rates (i.e., FRRF) are calculated as

$$JV_{PSII,abs} = \Phi_{RCII} \cdot F'_o \cdot K_a \cdot E \cdot 8.64 \times 10^{-8}, \quad (5)$$

where  $F'_o = (F_m \cdot F_0)/(F_m - F_0) \cdot (F'_q/F_m)$ .  $K_a = 11,800 \text{ m}^{-1}$  is an instrument-specific calibration factor,  $E = \text{irradiance} (\mu\text{mol photons m}^{-2} \text{ s}^{-1})$ , the factor  $8.64 \times 10^{-8}$  converts  $\mu\text{mol photons m}^{-2} \text{ s}^{-1}$  to  $\text{mol photons m}^{-2} \text{ d}^{-1}$  and  $\text{kg/m}^{-3}$  to  $\text{mg/m}^{-3}$ . The parameter  $\Phi_{RCII}$  ( $\text{mol e}^- \text{ mol photon}^{-1}$ ) has a constant value of 1, representing one electron transferred from P680 to quinone A ( $Q_A$ ) for each photon absorbed and delivered a reaction center (RCII) (Kolber & Falkowski, 1993). RCII was estimated as:

$$RCII = K_a \cdot F_0 / \sigma_{PSII}, \quad (6)$$

where  $F_0$  is dark-adapted base fluorescence and  $\sigma_{PSII}$  is the absorption cross-section area of the photosystem. As the RCII estimate might be biased by base fluorescence quenching during daytime,  $JV_{PSII}$  was corrected using an average RCII estimate from nighttime measurements (01:00–05:00 local).  $JV_{PSII}$  ( $\text{mol electrons m}^{-3} \text{ d}^{-1}$ ) was converted to carbon units using the conversion factor  $\Phi_{e:c}$  (Schuback & Tortell, 2019):

$$\Phi_{e:c} / \eta_{RCII} = 486 \cdot NPQ_{NSV} + 1854, \quad (7)$$

where  $\Phi_{e:c}$  is the electron generation to carbon fixation ratio,  $\eta_{RCII}$  is the RCII to Chl  $a$  ratio, and  $NPQ_{NSV}$  is the normalized Stern-Volmer nonphotochemical quenching coefficient. Since  $NPQ_{NSV}$  changed throughout the water column with changing light intensities,  $\Phi_{e:c}$  was variable. For simplicity, we used a literature value of 0.003 for  $\eta_{RCII}$  (Lawrenz et al., 2013) but recommend that  $\eta_{RCII}$  be measured directly on future cruises to avoid biasing estimates of  $\Phi_{e:c}$ . More detailed descriptions of the measured and calculated parameters and additional information for the production estimates using FRRF are provided in the Supporting Information (Table S1).

To calculate mixed-layer GPP from FRRF measurements, we used the in situ light attenuation from the CTD profile around noon to calculate the light field in the mixed layer over the diurnal cycle. The time-varying in situ light field was modeled using the empirical transmission-light attenuation relationship and surface PAR measured by the ship's meteorological system. Photosynthesis versus irradiance relationships were determined by fitting the productivity rate estimates from the FRRF versus the irradiance from the FRRF light curves using the Platt et al. (1980) definition:

$$\text{Productivity} = P_s \times \left[ 1 - e^{-\frac{\alpha E}{P_s}} \right] \times e^{-\frac{\beta E}{P_s}}, \quad (8)$$

where  $P_s$  equals the maximum photosynthesis,  $E$  equals the irradiance (PAR),  $\alpha$  is the initial slope of photosynthesis under low irradiance, and  $\beta$  is the slope under high/stressful irradiance. Additional methods on photophysiology including a table with the nomenclature is available in the Supporting Information (Methods S1 and Table S1).

### 3.8. Sediment Trap Deployments

We deployed VERTEX-style surface-tethered drifting sediment traps (Knauer et al., 1979) near the base of the euphotic zone. Trap crosspieces holding 12 acrylic tubes with an 8:1 aspect ratio, topped with baffles constructed of smaller beveled tubes, were deployed on a line with surface floats and a holey-sock drogue centered at 15-m depth. Tubes were deployed with a saltwater brine of filtered seawater and 0.4% formaldehyde. After recovery, overlying seawater was removed by gentle suction, and samples were analyzed under a dissecting microscope to remove mesozooplankton “swimmers.” Samples were then split on a Folsom splitter, filtered onto precombusted GF/F filters, acidified and analyzed for C, N, and isotopes on an isotope ratio mass spectrometer at the UC Davis Stable Isotope Facility. Previous comparisons with independent export flux estimates made using  $^{238}\text{U}$ - $^{234}\text{Th}$  disequilibrium approaches have shown no substantial overcollection or undercollection biases for our sediment trap configuration in the CCE (Stukel, Kahru, et al., 2019). For additional deployment and processing details, see Stukel, Kahru, et al. (2019).

### 3.9. Statistics

For all cycle data, variability was quantified as the standard errors of the means using the available 24-h integrated data. Since intracycle variability was a combination of measurement uncertainty and ecosystem variability, standard parametric statistics were not applicable. Throughout this manuscript, we present vertically integrated rates throughout the mixed layer, unless otherwise stated. For bottle samples, we used trapezoidal integration. For the  $\text{NPP}_{14\text{C}}$  algorithm used for the P1706 cruise, uncertainties in parameter estimates were propagated through all equations.

## 4. Results

### 4.1. General Features of the Two Cruises

Four different regions were sampled during the P1604 cruise (Figure 1): the offshore stratified region (P1604-C1), the core of the California Current (P1604-C2), offshore of the coastal boundary in the wind stress curl upwelling domain (P1604-C3), and the coastal boundary upwelling region (P1604-C4). Over the course of four cycles on P1706, we followed upwelled waters from nearshore to offshore. P1706-C1 was located in freshly upwelled waters; P1706-C2 started ~77 km NW of the end of P1706-C1 in partially aged upwelled waters; and P1706-C3 began ~140 km southwest of the start of P1706-C2 in postbloom waters. Postcruise analysis indicated that P1706-C3 was not part of the main filament and contained water characteristic of the California Current, likely advected from the North. P1706-C4 was a continuation of P1706-C2 initiated about 26 km northeast of the start of P1706-C3 (Figure 1). Average mixed-layer depth, temperature, Chl  $a$ , and nutrient concentrations are given in Table S2 for all cycles. Full data are available in the CCE-LTER database: [https://oceaninformatics.ucsd.edu/datazoo/catalogs/ccelter/datasets?fc=11:29820ps20=1:0\\_2:0\\_3:0\\_9:0\\_11:0](https://oceaninformatics.ucsd.edu/datazoo/catalogs/ccelter/datasets?fc=11:29820ps20=1:0_2:0_3:0_9:0_11:0).

### 4.2. Phytoplankton Production

#### 4.2.1. $^{14}\text{C}$ Primary Production

$^{14}\text{C}$ -derived estimates of NPP are from field incubations conducted during P1604 and from a general algorithm based on CCE field incubations for P1706 (Stukel, Goericke, & Landry, 2019). Both are defined as  $\text{NPP}_{14\text{C}}$  and treated the same.

$\text{NPP}_{14\text{C}}$  decreased slightly between successive days during P1604-C2 (22, 17 and 14  $\text{mmol C m}^{-2} \text{d}^{-1}$ ), increased daily during P1604-C3 (36, 45, and 64  $\text{mmol C m}^{-2} \text{d}^{-1}$ ), and had the highest rates (150, 103, and 113  $\text{mmol C m}^{-2} \text{d}^{-1}$ ) during P1604-C4 (Figure 3, Table S4). A strong gradient of decreasing  $\text{NPP}_{14\text{C}}$  with distance from shore is therefore evident in the P1604 data.

$NPP_{14C}$  for P1706 showed a wider range of results but a similar decrease from nearshore to offshore (Figure 4, Table S4). In freshly upwelled waters during P1706-C1, production tripled from 220  $\text{mmol C m}^{-2} \text{d}^{-1}$  for Day 1 (D1) to 718 and 596  $\text{mmol C m}^{-2} \text{d}^{-1}$  for D2 and D3, respectively. In P1706-C4 offshore waters, average  $NPP_{14C}$  was 30-fold lower (13 and 19  $\text{mmol C m}^{-2} \text{d}^{-1}$  for D1 and D2, respectively). Between these extremes,  $NPP_{14C}$  varied from  $\sim 250$  to 300  $\text{mmol C m}^{-2} \text{d}^{-1}$  during P1706-C2 and decreased from  $\sim 90$  to 48  $\text{mmol C m}^{-2} \text{d}^{-1}$  from D1 to D3 during P1706-C3.

#### 4.2.2. $NPP_{G/G}$ From Dilution Growth and Grazing Rates

$NPP_{G/G}$  estimates closely follow the magnitudes and trends observed for  $NPP_{14C}$  (Table 1). Mean rates are higher for P1604-C3 compared with C2 ( $48.4 \pm 8.4$  vs.  $17.7 \pm 4.5$   $\text{mmol C m}^{-2} \text{d}^{-1}$ ) and decrease even further to 9.4  $\text{mmol C m}^{-2} \text{d}^{-1}$  during P1604-C1. For P1604-C2, day-to-day  $NPP_{G/G}$  variability (44, 24, and 36  $\text{mmol C m}^{-2} \text{d}^{-1}$  for D1–D3, respectively) is similar to that of NP and NPP measurements. During P1604-C3,  $NPP_{G/G}$  increased from 49 to 76  $\text{mmol C m}^{-2} \text{d}^{-1}$  over the 3-day occupation, similar to the increase in independently measured  $NPP_{14C}$ . While no  $NPP_{G/G}$  data were obtained for the nearshore P1604-C4, the high rates were found in the freshly upwelled waters of P1706-C1 ( $511 \pm 150$   $\text{mmol C m}^{-2} \text{d}^{-1}$ ; range 252 to 588  $\text{mmol C m}^{-2} \text{d}^{-1}$ ). Over subsequent P1706 experiments,  $NPP_{G/G}$  decreased each day along the upwelling filament, averaging  $270 \pm 44$ ,  $76 \pm 39$  and  $22 \pm 6$   $\text{mmol C m}^{-2} \text{d}^{-1}$  for Cycles 2 to 4, respectively.

#### 4.2.3. NP ( $^{15}\text{NO}_3$ Uptake)

Mixed-layer integrated rates of nitrate-based NP are given in Table 1 as carbon equivalents using a N:C conversion of 6.625. For P1604, mean NP rates of  $11 \pm 3$   $\text{mmol C m}^{-2} \text{d}^{-1}$  during offshore Cycle 2 increased to  $24 \pm 8$  and  $23 \pm 6$   $\text{mmol C m}^{-2} \text{d}^{-1}$ , respectively, during Cycles 3 and 4. For P1706, NP was highest ( $157 \pm 19$   $\text{mmol C m}^{-2} \text{d}^{-1}$ ) in C1 upwelled waters and declined progressively during offshore filament transport. NP averaged  $101 \pm 44$   $\text{mmol C m}^{-2} \text{d}^{-1}$  during P1706-C2, but decreased by 75% from days D1 and D2 to D3 (Table S4). Further offshore, NP decreased to  $29 \pm 18$  and  $5 \pm 0.1$   $\text{mmol C m}^{-2} \text{d}^{-1}$  during C3 and C4, respectively.  $f$  ratios (the ratio of new to total production, estimated as  $\text{NP}/NPP_{14C}$ ) varied from 0.2 to 0.7 over all experiments but lacked a consistent onshore-offshore trend (Table 1).

#### 4.2.4. Net Community Production ( $NCP_{\text{prior}}$ )

Conventional  $\text{O}_2/\text{Ar}$ -NCP estimates in complex systems such as the CCE are challenging to interpret. Our companion paper (Wang et al., 2020) discusses these shortcomings along with method improvements used to estimate NCP more reliably in the present field campaigns. Here, we use these new insights in discussing the traditional NCP analysis ( $NCP_{\text{prior}}$ ) and a real-time NCP ( $NCP_{\text{inst}}$ ), which integrate  $\text{O}_2/\text{Ar}$  signals over different time scales. The  $\text{O}_2$  residence time, as determined by wind speed reanalysis and mixed-layer depth was between 6.6 and 15.6 days for P1604 and between 2.6 and 9.0 days for P1706 (Wang et al., 2020; Figure 2). During both cruises, the heterogenous nature of NCP in the CCE-LTER region is indicated by significant short- and long-term trends in  $NCP_{\text{prior}}$  (Figures 3 and 4).

$NCP_{\text{prior}}$  was steady and low during P1604-C2 and highest during P1694-C4 ( $5.5 \pm 0.3$  and  $39.5 \pm 4.0$   $\text{mmol C m}^{-2} \text{d}^{-1}$ , respectively; Table 1). Although the water mass appeared well equilibrated with the atmosphere during P1604-C3,  $NCP_{\text{prior}}$  changed from slightly net heterotrophic at the beginning of the cycle ( $-10.7$   $\text{mmol C m}^{-2} \text{d}^{-1}$ ) to slightly net autotrophic ( $8.6$   $\text{mmol C m}^{-2} \text{d}^{-1}$ ) at the end, averaging  $-0.3 \pm 5.6$   $\text{mmol C m}^{-2} \text{d}^{-1}$ .  $NCP_{\text{prior}}$  showed clear diurnal amplitudes during P1604-C2 and C4, with increasing rates during daylight and decreasing rates at night (Figure 3). The diurnal amplitude was, however, less pronounced during P1604-C3.

#### 4.2.5. Real-Time Analysis of NCP ( $NCP_{\text{inst}}$ )

Real-time analysis of NCP data ( $NCP_{\text{inst}}$ ) accounts mainly for  $\text{O}_2/\text{Ar}$  change over the previous 1 h, including the instantaneous gas exchange coefficients. The system was net autotrophic for P1604-C2 and C4, decreasing from 9.7 to 1.1  $\text{mmol C m}^{-2} \text{d}^{-1}$  over the duration of C2 (Table S4) and subsequently increasing to  $16.4 \pm 4.0$   $\text{mmol C m}^{-2} \text{d}^{-1}$  for C4 (Tables 2 and S4).  $NCP_{\text{inst}}$  indicates a slightly net heterotrophic system ( $-0.1 \pm 1.2$   $\text{mmol C m}^{-2} \text{d}^{-1}$ ) during P1604-C3.

$NCP_{\text{inst}}$  estimates were net autotrophic for P1706-C1 ( $77.8 \pm 0.5$   $\text{mmol C m}^{-2} \text{d}^{-1}$ ) and net heterotrophic for P1706-C2 ( $-14.3 \pm 11.3$   $\text{mmol C m}^{-2} \text{d}^{-1}$ ). For Cycles 3 and 4, the signals were strongly affected by ship movements through other waters mixed in with the relatively narrow filament. Consequently, we view these  $NCP_{\text{RT}}$  estimates as unreliable and do not discuss them further.



**Table 1**  
Production Metrics for California Current Ecosystem Long-Term Ecological Research Process Cruises P1604 and P1706

	NCP prior	NCP inst	NPP <sub>14C</sub>	NPP G/G	NP	Export flux	f-ratio	GPP (FRRF)	GPP-EIMS	Respiration (EIMS)
<i>P1604</i>										
Cycle 2	5.51 ± 0.25	6.02 ± -0.13	17.7 ± 4.5	35.0 ± 5.8	10.6 ± 2.7	3.4	0.55 ± 0.06	ND	42.25 ± 9.3	57.25 ± 3
Cycle 3	-0.59 ± 5.61	-0.13 ± 1.18	48.4 ± 8.4	61.9 ± 7.8	23.9 ± 8.0	10.0	0.44 ± 0.07	ND	124 ± ND	131 ± ND
Cycle 4	39.47 ± 3.99	16.37 ± 4.04	126.4 ± 23.4	ND	22.9 ± 5.9	20.9	0.16 ± 0.01	ND	348 ± 158	418.35 ± 190.16
<i>P1706</i>										
Cycle 1	58.89 ± 1.24	77.84 ± 0.5	511.5 ± 150.1	524.1 ± 142.1	156.8 ± 19.2	29.3	0.34 ± 0.09	767.2 ± 148	1082 ± 134	1278.67 ± 76.93
Cycle 2	-12.23 ± 8.57	-14.26 ± 11.32	256.3 ± 27.9	269.2 ± 44.1	101.6 ± 44.0	44.5	0.40 ± 0.14	502.9 ± 92	401.1 ± 52.3	554.25 ± 101.32
Cycle 3	-11.8 ± 33.05	-10.47 ± 4.29	70.4 ± 21.9	76.7 ± 39.1	29.3 ± 18.5	46.7	0.49 ± 0.26	92.4 ± 12.8	X	X
Cycle 4	-0.19 ± 1.16	-0.07 ± 0.28	18.5 ± ND	22.00 ± 6.4	5.4 ± 0.1	35.7	0.27 ± X	31.2 ± 1.4	X	X

Note. Values represent average rates in mmol C m<sup>-2</sup> d<sup>-1</sup> integrated over the mixed-layer depth. Errors are standard errors of the mean (SOM). ND indicates that no measurements were made. X indicates that data were not reliable as indicated in the text.

#### 4.2.6. GPP Based on NCP (GPP<sub>O<sub>2</sub>/Ar</sub>)

GPP<sub>O<sub>2</sub>/Ar</sub> averaged 42 ± 9 and ~ 130 mmol C m<sup>-2</sup> d<sup>-1</sup> for P1604-C2 and C3, respectively. No error determination could be made for C3 as the respiration measurements during Days 1 and 2 were positive values when the ship moved through different water masses; hence, only Day 3 date could be used for this cycle. High GPP<sub>O<sub>2</sub>/Ar</sub> rates were estimated for nearshore cycles P1604-C4 (4348 ± 171 mmol C m<sup>-2</sup> d<sup>-1</sup>) and P1706-C1 (1082 ± 134 mmol C m<sup>-2</sup> d<sup>-1</sup>). For P1706-C2, estimated GPP declined to 401 ± 52 mmol C m<sup>-2</sup> d<sup>-1</sup>. As noted above, estimates for P1706-C3 and C4 were compromised by ship movements through mixed waters.

#### 4.2.7. GPP<sub>FRRF</sub> Estimates

No FRRF measurements were conducted during P1604. For P1706, mean GPP<sub>FRRF</sub> estimates declined progressively following along onshore-to-offshore filament transport of upwelled water from 762 ± 148 to 502 ± 92.8 μg C m<sup>-2</sup> d<sup>-1</sup> for C1 and C2, respectively, to 92.4 ± 13 and 31 ± 1 μg C m<sup>-2</sup> d<sup>-1</sup>, for C3 and C4 (Figure 4f, Table 1). For P1706-C1, diurnally averaged GPP increased with time spent in the water mass (519 to 1148 μg C m<sup>-2</sup> d<sup>-1</sup> for D1 to D3; Table S4). For other P1706 cycles, GPP was relatively constant or decreased slightly (Table S4). As shown in Figure 4, GPP rates showed a distinct diurnal periodicity with notably higher rates during the noon/afternoon hours. Spikes during P1706-C1 and C2 are most associated with occasional net tows when the ship briefly left the drift array and entered water parcels with higher surface Chl *a*.

### 4.3. Photophysiology and Light Acclimation

The maximum quantum yield (F<sub>v</sub>/F<sub>m</sub>) of the dark-adapted phytoplankton community for P1706-C1 was around 0.48 to 0.5 during nighttime and morning hours but dipped to ~0.4 at the end of the photoperiod of D2 and D3 (Figure S1). Values of ~0.5 are the maximum measurable in nonstressed cells using single turnover measurements with our FRRF instrument. For P1706-C2, F<sub>v</sub>/F<sub>m</sub> was lower (0.39–0.42) during night and morning hours, but also showed a relative decline towards the end of each photoperiod. F<sub>v</sub>/F<sub>m</sub> increased steadily from 0.4 to ~0.49 during P1706-C3 but was relatively constant (~0.45) for P1706-C4. Both of these cycles (C3 and C4) were dominated by smaller phytoplankton, mainly cyanobacteria, and neither displayed the distinct diel decreases in F<sub>v</sub>/F<sub>m</sub> as seen in C1 and C2. The absorption cross-sectional area of PSII (σ) did not show a diel pattern, yet, σ was enhanced during C2 (6 nm<sup>2</sup> PSII<sup>-1</sup>) compared with C1 (4–5 nm<sup>2</sup> PSII<sup>-1</sup>). For C3, σ was 6 nm<sup>2</sup> PSII<sup>-1</sup> while in C4, the absorption cross-sectional area of PSII was 5.5 nm<sup>2</sup> PSII<sup>-1</sup>. 1/τ decreased throughout the light phase and increased during the dark period. This pattern was well defined in C1 and C2, dampened in C3, and nonexistent in C4. Compared with C1, 1/τ increased in our C2 measurements. Enhanced NPQ<sub>NSV</sub> rates (data not shown) were also measured in C2. Parameters derived from the fluorescence induction curves (α, P<sub>max</sub>) showed some variability within and between cycles. Maximum photosynthetic electron transport (P<sub>max</sub>) increased towards the ends of each photoperiod in C1 and C2, but was relatively constant for C3 and C4 (Figure S1). α did not show diel changes, yet, values for C1 and C2 were significantly lower compared with C3 and C4. The light saturation point (E<sub>K</sub>) (averages, including light and dark phase, were 427 ± 106 for C1, 389 ± 203 for C2, 555 ± 143 for C3, and 583 ± 133 for C4). Those values are much higher than mean mixed-layer daytime light intensities, which averaged 151, 170, 140, and 329 μmol photons m<sup>-2</sup> s<sup>-1</sup> for C1–C4, respectively. Light intensity and E<sub>K</sub> were not correlated. Similarly, no change in the initial slope (α) was observed with changes in mean daytime light intensity.

### 4.4. Export Flux

Sediment trap-measured export near the base of the euphotic zone decreased with distance from shore on the P1604 cruise, with values of 20.9, 10.0, and 3.4 mmol C m<sup>-2</sup> d<sup>-1</sup> for coastal C4, transition C3, and offshore C2, respectively (Figure 3). Export efficiency, however, remained relatively constant with distance from shore on this cruise. The *e* ratio (defined as export/NPP<sub>14C,eup</sub>, where NPP<sub>14C,eup</sub> is NPP<sub>14C</sub> integrated to the base of the euphotic zone) was 0.15, 0.14, and 0.15 for C2–C4, respectively. In contrast, export near the base of the euphotic zone showed

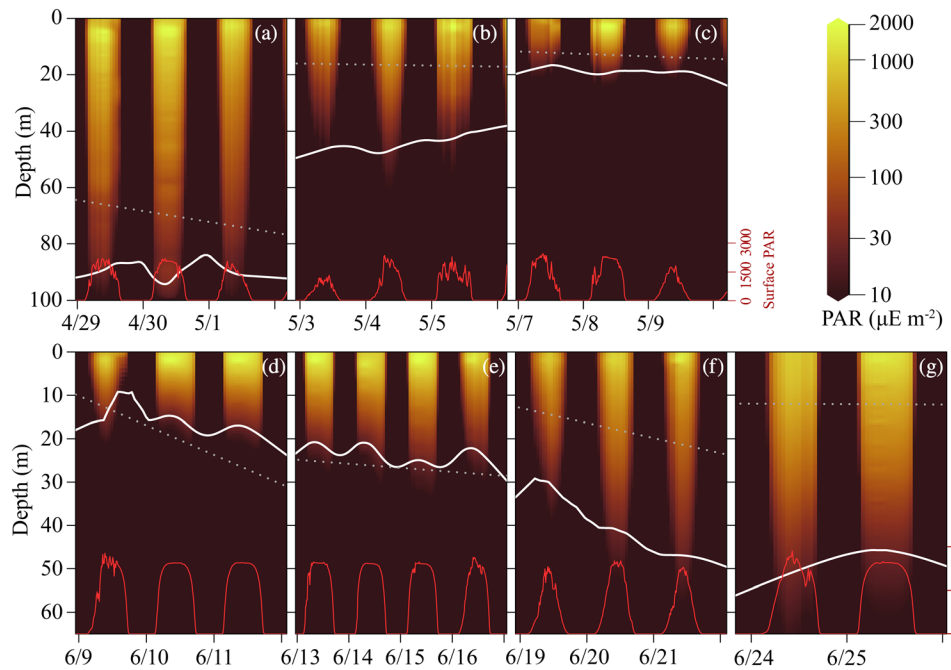


**Figure 2.** Mixed-layer depth and light levels for all experimental cycles. (a) P1604-C2, (b) P1604-C3, (c) P1604-C4, (d) P1706-C1, (e) P1706-C2, (f) P1706-C3, and (g) P1706-C4. Red lines indicate surface PAR intensity, colored shading indicate water column light intensity ( $\mu\text{mol photons m}^{-2} \text{s}^{-1}$ ), white solid line indicates depth of the 1% light level, and dotted line indicates the mixed-layer depth.

no clear trend with distance from shore on P1706. Sinking flux was  $29.3 \text{ mmol C m}^{-2} \text{ d}^{-1}$  in the coastal C1,  $44.5 \text{ mmol C m}^{-2} \text{ d}^{-1}$  in the early filament C2,  $35.7 \text{ mmol C m}^{-2} \text{ d}^{-1}$  in the late filament C4, and  $46.7 \text{ mmol C m}^{-2} \text{ d}^{-1}$  in transition water C3 (Figure 4). This led to an inverse relationship between mixed-layer Chl *a* and the *e* ratio, with *e* ratios of 0.05, 0.18, 0.43, and 0.79 for C1–C4, respectively.

#### 4.5. Inter-cruise and Intra-cruise Variability in Production Relationships

Cycle P1604-C2 started in the core of the California Current, and NP was matched by modest NCP values and a diel pattern in the  $\text{dO}_2/\text{Ar}$  measurements (Figures 3j and 3l). Overall, P1604-C2 was moderately net autotrophic, but due to the partial depletion of nutrients and change in weather conditions, most production measures showed reduced rates towards the end of the cycle. For P1604-C3, offshore of the coastal boundary in the wind stress curl upwelling domain, NPP and NP-based estimates increased significantly compared with C2, yet  $\text{NCP}_{\text{prior}}$  was negative at the beginning of the cycle, but became positive around D3. This change in production was correlated with a change in weather as the sea became much calmer and cloud cover was reduced. As expected, productivity was highest in the coastal upwelling region (P1604-C4), where carbon-based production rates tripled. Despite high  $\text{NO}_3^-$  concentrations, the phytoplankton appeared to utilize  $\text{NH}_4^+$  primarily for growth.  $\text{NCP}_{\text{prior}}$  during P1604 indicated that the system was strongly net autotrophic.

Productivity was high where nutrients were plentiful close to shore in the freshly upwelled water of P1706-C1. However, overcast light conditions reduced productivity estimates (except  $\text{NCP}_{\text{prior}}$ ) during the early part of this cycle. Comparatively low NP:NPP rate estimates indicate that the phytoplankton community used both ammonia and nitrate as N sources.  $\text{NCP}_{\text{prior}}$  rates averaged 50% of NP, but a distinct diel pattern was observed. P1706-C2 showed reduced production compared with C1, as a result of reduced chlorophyll concentration. Despite lower NPP, NP was higher on Day 1 of C2 compared with C1. NCP analysis indicated that the watermass started to become net heterotrophic at the end of this cycle. P1706-C3 was conducted in a region just outside of the filament where water from the California Current mixed with filament water. P1706-C3 was initially net autotrophic, but production rates were strongly reduced compared with C1 and C2. The continuous negative trend in NCP was likely driven by horizontal and vertical

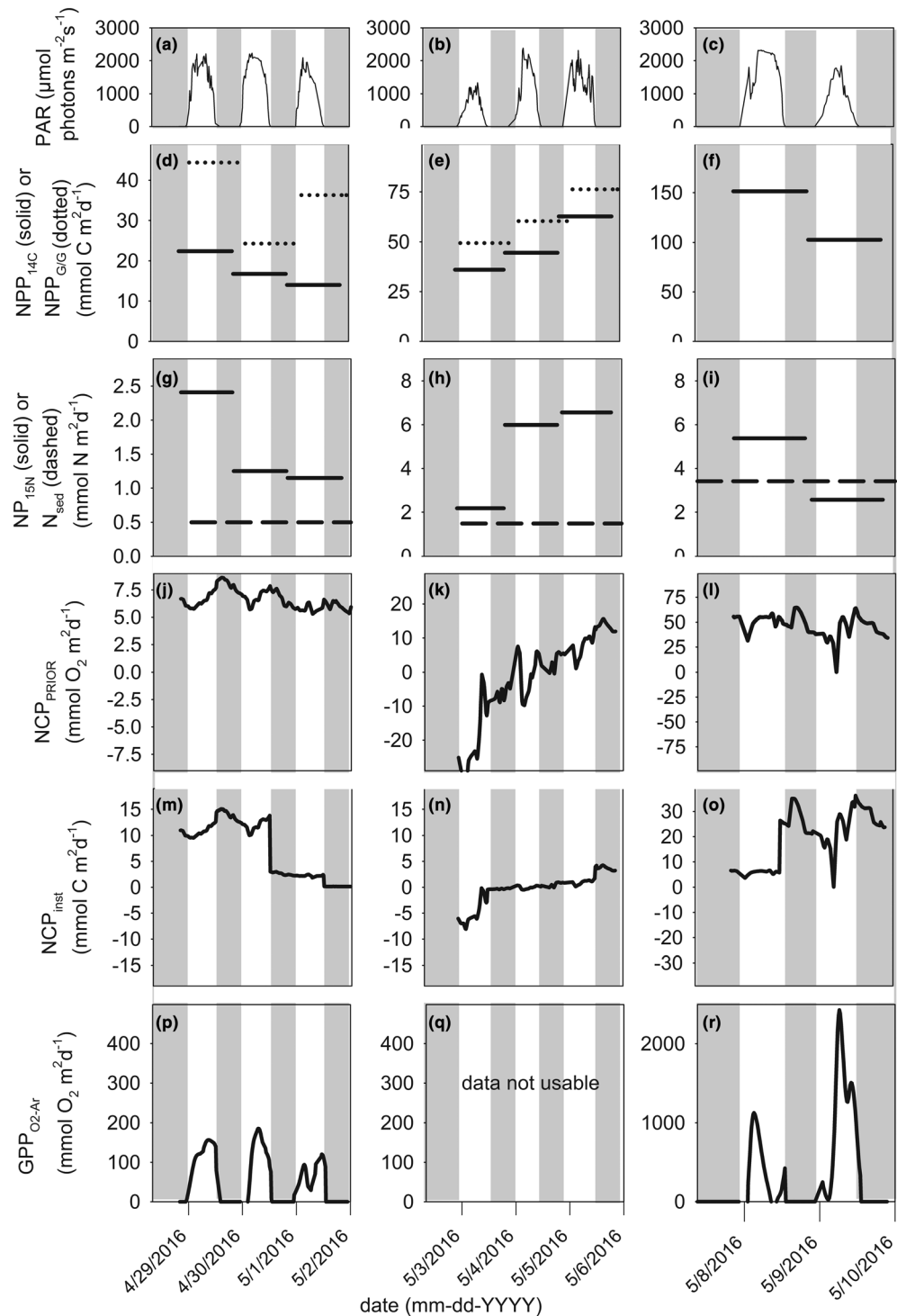


**Figure 3.** Chronology of primary production estimates during P1604. Panels (a–c) depict light intensity during P1604-C2, C3, and C4, respectively. Panels (d–f) represent NPP derived from  $^{14}\text{C}$  incubations (solid lines) and NPP<sub>G/G</sub> from dilution incubations (dashed lines). Panels (g–i) show new production (from  $^{15}\text{N}$  incubations; solid lines) and export production from sediment traps (dashed lines). Panels (j–l) show mixed layer NCP<sub>Prior</sub>. Panels (m–o) show instantaneous air-sea biological  $\text{O}_2$  flux. Panels (p–r) represent calculated GPPs during the diel cycles as measured by NCP<sub>inst</sub>. Note changes in scales and units as indicated by the axis labels. Data in panels (d–i) are integrated over 24 h and mixed-layer depth. Data in panels (a–c) and (j–r) are integrated over 30-min intervals. Please note that data in panel m and o have been disproportionately affected by a sudden change in wind speed, a corresponding k value, and hence resulted in a step in NCP<sub>inst</sub> values.

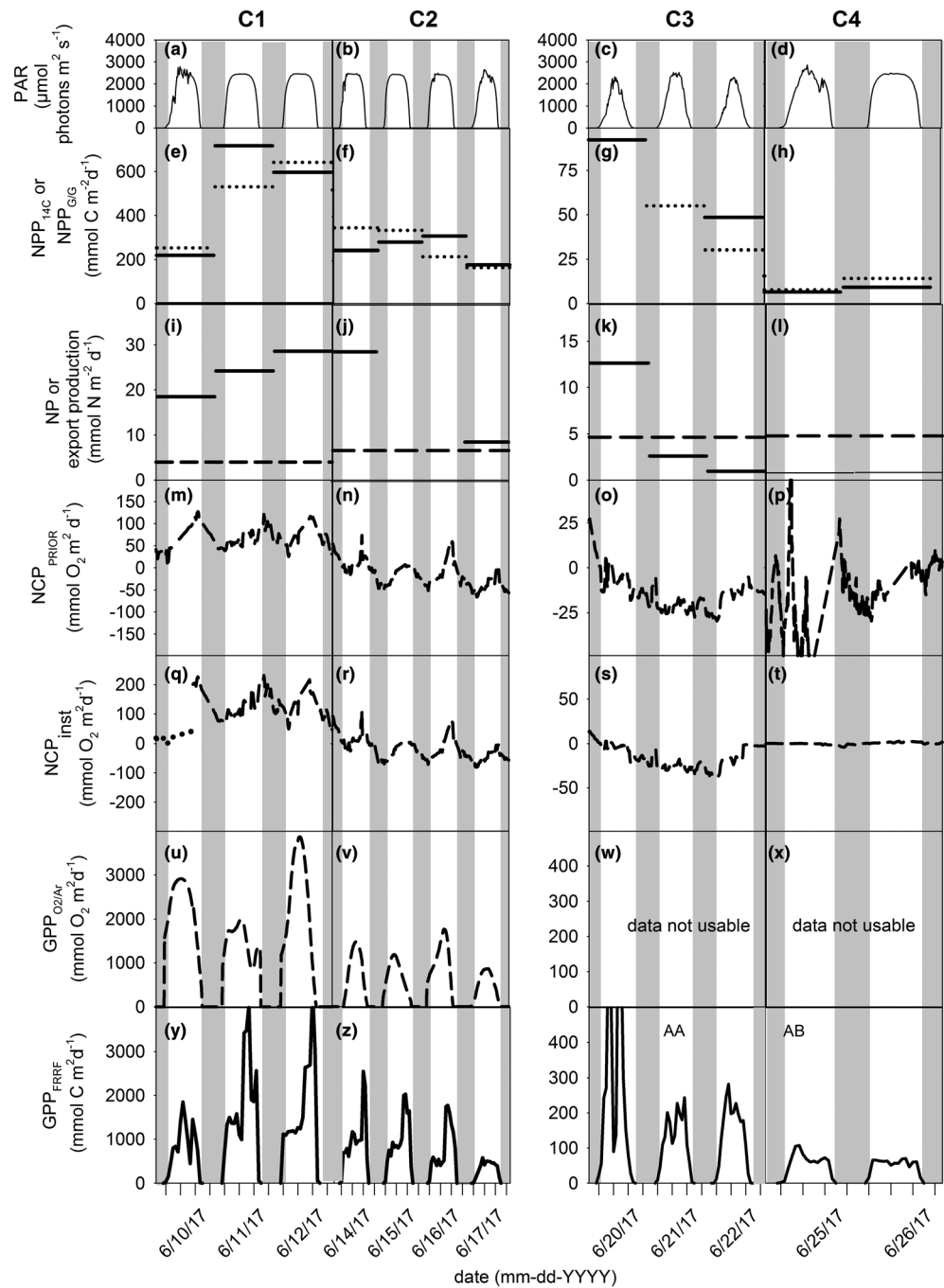


**Figure 4.** Chronology of primary production estimates during P1706. Panels (a–d) depict the light intensity during the for cycles P1706-C1 to C4, respectively. Panels (e–h) represent NPP derived from  $^{14}\text{C}$  incubations (solid lines) and the  $\text{NPP}_{\text{G/G}}$  from dilution incubations (dashed lines). Panels (i–l) show net production (from  $^{15}\text{N}$  incubations) and export production from sediment traps. Panels (m–p) represent net community production measured with weighted  $k$ . Panels (q–t) show net community production calculated using instantaneous  $k$ . Panels (u–x) represent calculated gross primary production from instantaneous NCP. Panels (y–ab) represent gross primary production measured by FRRF. Note changes in scales and units as indicated by the axis labels. Data in panels (e–p) are integrated over 24 h and the mixed-layer depth. Data in panels (a–d) and (m–ab) are integrated over 30-min intervals. Please note that data of cycle 1\_1 (dotted line in panel q) have been disproportionately affected by a sudden drop in wind speed, a corresponding  $k$  value, which explains the sharp step in  $\text{NCP}_{\text{inst}}$  values.

mixing of different water masses, a deepening of the mixed-layer depth over time (Figure 2) and the observed decrease of Chl *a* during this cycle (Figure S2). P1704-C4 was conducted at the location of a drifter that marked the water parcel sampled during C2 and can thus be considered an extension of the previous filament cycle. It was characterized by low chlorophyll despite a nitrate concentration of around 2.9  $\mu\text{M}$  and an ammonium concentration of 1.7  $\mu\text{M}$ . The extremely low NP and the low *f* ratio (0.24) also indicate that the phytoplankton community was taking up mostly regenerated N. Further analysis (see section 5 below) indicated that Cycle 2 was iron limited. NCP rates were found to be near air saturation, indicating that autotrophic and heterotrophic processes were in balance despite the elevated ammonium.

#### 4.6. Production Comparison

We had two independent estimates of GPP ( $\text{GPP}_{\text{FRRF}}$  and  $\text{GPP}_{\text{O}_2/\text{Ar}}$ ), two independent estimates of NPP ( $\text{NPP}_{14\text{C}}$  and  $\text{NPP}_{\text{G/G}}$ ), and three estimates of NCP or NP ( $\text{NCP}_{\text{prior}}$ ,  $\text{NCP}_{\text{RT}}$ , and nitrate uptake). The independent GPP experiments can only be compared for two cycles (P1706-C1 and P1706-C2) because FRRF measurements were not made on the P1604 cruise and because ship movements in and out of the mesoscale filament invalidated  $\text{GPP}_{\text{O}_2/\text{Ar}}$  assumptions for P1706-C3 and C4. Nonetheless, there is reasonable agreement between the two methods. On P1706-C1, the ratio of  $\text{GPP}_{\text{FRRF}}:\text{GPP}_{\text{O}_2/\text{Ar}}$  was 0.75, and on P1706-C2 it was 1.25. Agreement was even better for the two NPP measurements, yielding a Pearson's linear correlation of 0.9997 ( $\rho < 10^{-5}$ ). The mean  $\text{NPP}_{14\text{C}}$  across all paired cycles was 214  $\text{mmol C m}^{-2} \text{d}^{-1}$ , while the mean  $\text{NPP}_{\text{G/G}}$  was 223  $\text{mmol C m}^{-2} \text{d}^{-1}$ . Comparing mean NPPs to mean GPPs for P1706-C1 and C2 (941 and 465  $\text{mmol C m}^{-2} \text{d}^{-1}$  for C1 and C2, respectively), the resulting NPP:GPP ratios are 0.55 and 0.56, respectively, suggesting that 55% of phytoplankton GPP, on average, goes to biomass production. Compared with the agreement between alternate GPP or NPP measurements, the correlation between  $\text{NCP}_{\text{prior}}$  and  $\text{NCP}_{\text{inst}}$  is weak and not statistically significant (Pearson's  $\rho = 0.60$ ,  $p = 0.15$ ). This discrepancy was expected, however, as it reflects the different temporal integration scales of  $\text{NCP}_{\text{prior}}$  and  $\text{NCP}_{\text{inst}}$  and the substantial differences in NCP observed in the P1706 filament. There is also substantial discrepancy between NP and the two NCP estimates. The strongest correlation is between NP and  $\text{NCP}_{\text{prior}}$ , though not statistically significant ( $\rho = 0.52$ ,  $p = 0.24$ ). NP measurements also substantially exceed those of  $\text{NCP}_{\text{prior}}$  and  $\text{NCP}_{\text{RT}}$ , where mean  $\text{NCP}_{\text{prior}}$  is 8.7  $\text{mmol C m}^{-2} \text{d}^{-1}$  and mean NP is 73  $\text{mmol C m}^{-2} \text{d}^{-1}$ .

### 5. Discussion

The P1604 and P1706 cruises both aimed to measure ecosystem dynamics and biogeochemical rates. The Lagrangian sampling plan and multimethod approach allowed us to compare a number of different productivity estimates over a broad range of environmental conditions. P1604 occurred near the end of an anomalously warm period in the northeast Pacific that began with the 2014–2015 North Pacific heat wave and continued with an El Niño in 2015–2016 (Bond et al., 2015; Jacox et al., 2016). At the time of this cruise, much of the region remained above normal temperatures, but upwelling had resumed along the coast, leading to phytoplankton blooms during nearshore experiments P1604-C3 and C4. P1706 aimed to follow filament transport of freshly upwelled water offshore. Due to this mesoscale focus, P1706 cruise results are substantially influenced by (1) rapid changes in water column properties over time; (2) mixing of upwelled and offshore waters during transport; and (3) small-scale spatial gradients in the vicinity of the drift array. In the following discussion, we consider the compatibility and differences among multiple primary production measurements and their applicability in this dynamic region. To compare productivity rate estimates, all data are integrated over the same temporal scale (24 h, cycle duration), analyzed over the mixed-layer depth, and normalized to carbon units.

#### 5.1. $\text{GPP}_{\text{FRRF}}$ and $\text{GPP}_{\text{O}_2/\text{Ar}}$ Comparisons to NPP

Only recently has it been possible to measure GPP rates with high temporal resolution during research cruises (Hamme et al., 2012; Schuback & Tortell, 2019). Here, we used GPP estimates based on underway FRRF measurements and rates derived from  $\text{O}_2/\text{Ar}$  data. We modified the FRRF method described by Oxborough et al. (2012) to account for potential biases such as noontime fluorescence quenching and flexible chlorophyll-to-carbon fixation ratios (Schuback et al., 2018). The broader suite of potential corrections as suggested by Boatman et al. (2019) and Schuback et al. (2018) was not available to us during this study. The FRRF data were subsequently compared with the  $\text{NCP}_{\text{O}_2/\text{Ar}}$  data from which GPP rates were

calculated. As the NCP approach is based on changes of  $O_2$  concentration in the water column, a photosynthetic quotient (PQ; oxygen evolved to carbon fixed) was applied to convert rates into carbon units. Generally, a PQ of 1.4 for  $NO_3^-$  supported production and 1.1 for  $NH_4^+$  supported production is used. However, for simplicity and as the PQ can also vary with light induced stress (Iriarte, 1999) as well as other stress factors (Spilling et al., 2015), we used a PQ of 1.2 for all samples. Changes in  $O_2/Ar$  include all photoautotrophic and heterotrophic activity. Hence, a positive trend during the day indicates that photoautotrophy outweighs all chemoheterotrophy, including phytoplankton respiratory processes. Daytime production includes all respiratory processes and photosynthesis while nighttime data measure only respiratory processes. In order to estimate GPP from diel cycles in  $O_2/Ar$ , we assume that the nighttime and daytime respiration rates are equal.

Since no FRRF measurements were conducted during the P1604 cruise, GPP rates were only obtained using the  $O_2/Ar$  data. The diurnal rate estimates followed distinct diurnal cycles with a maximum production of around  $160 \text{ mmol C m}^{-2} \text{ d}^{-1}$  and a daily average around  $40 \text{ mmol C m}^{-2} \text{ d}^{-1}$ . As noted by Landry et al. (2011a), carbon-based phytoplankton production measured from dilution experiments exceed those from  $NPP_{14C}$  because they separately account for phytoplankton biomass growth and production grazed by microzooplankton over the course of 24-h incubations while  $NPP_{14C}$  incorporates respiration losses of grazed  $^{14}C$ -labeled carbon into the measurement. Hence, the difference in portions of GPP recovered by  $NPP_{14C}$  and  $NPP_{G/G}$  might be interpreted as measure of production losses during transfer of the organic matter through the food web. P1706-C1 and C2 gave high GPP rates for both  $O_2/Ar$  and FRRF, with daily midday maxima  $>3,000 \text{ mmol C m}^{-2} \text{ d}^{-1}$  for C1 and  $>1,000 \text{ mmol C m}^{-2} \text{ d}^{-1}$  C2. Direct comparison of cycle means indicates that rates were not statistically significantly different between methods ( $p \geq 0.4$ ,  $t$  test, Mann-Whitney rank sum test).  $GPP_{O_2/Ar}$  for P1706-C3 and C4 were compromised by the ship passing through different water masses frequently, which precluded calculating day and night rates for the same water parcel. GPP rates were nonetheless obtained for those cycles from FRRF data. Comparing  $NPP_{14C}$  and  $GPP_{FRRF}$  estimates for all cycles showed a reasonable percent of carbon loss: 36%, 51%, 27%, and 40% of GPP for P1706-C1–C4, respectively. For the CCE region,  $\sim 20\%$  of fixed carbon is released to the DOC pool, with a range between 7% and 44% (Goericke unpublished data; Stukel et al., 2012). Respiration alone can also reduce NPP on average by 9% to 22% (López-Sandoval et al., 2014). Higher as well as lower ratios of  $NPP:GPP$  have been reported in literature (e.g., Bercel & Kranz, 2019; Kranz et al., 2010). In addition, measured  $O_2$ -based GPP estimates that are  $>200\%$  of simultaneous NPP measurements have been reported in field studies (Hashimoto et al., 2005; Laws et al., 2000). Hence, our  $NPP/GPP$  ratios fall within expected ranges.

Some uncertainties of the  $GPP_{FRRF}$  merit discussion. The  $GPP_{FRRF}$  analysis is based on daytime  $P$  versus  $E$  curves, but estimates of the photosystem reaction centers (RCII) come from nighttime sampling. Since the number of functional RCII varies throughout the day, overestimates or underestimates of rates may occur. In addition, our calculated GPP rates for the photic zone come solely from phytoplankton sampled at 5- to 10-m depth. Despite dark or low-light acclimation prior to measurements, the photosystem might not have had time to reoxidize fully, resulting in underestimates of quantum yield and photochemical production. Moreover, surface communities might express different values in photosynthetic efficiency under low light intensities ( $\alpha$ ) and maximum photosynthetic rates compared with deep samples. This bias is apparent when analyzing the relatively fast diel changes (Figure S1), which are likely faster than cell mixing in the water column. Hence, if deeper cells are better adapted to low-light conditions, calculated rates from the mixed layer might be underestimated. Nonetheless, since the MLD was relatively shallow for most cycles (Figure 2), we expect a relatively good estimate. Part of the temporal and spatial mismatch between  $GPP_{FRRF}$  and  $GPP_{EIMS}$  might also be explained by likely changes in the electron to C ratios occurring throughout the day, which could partially decouple  $O_2$  production from C fixation. Lastly, due to the lack of pigment data, no spectral correction could be applied to our rate estimates (Schuback et al., 2018). Despite these shortcomings, the good agreement between FRRF and  $O_2/Ar$  methods gives us some confidence that both approaches can reliably estimate water column GPP.

As changes in production are associated with the ability of phytoplankton to efficiently utilize light or dissipate excess light, photophysiological parameters as presented in (Figure S1) can add a more mechanistic understanding of some of the presented production rates. A significant change in photophysiological

responses was seen in the data for P1706-C2. The observed drop in maximum quantum yield ( $F_v/F_m$ ) indicates conditions that negatively affect photosystem function in the phytoplankton community, such as iron (Fe) limitation. Iron limitation is associated not only with a loss in quantum yield efficiency but also, more importantly, the optical absorption cross section of the photosystem ( $\sigma$ ), the area of chlorophyll pigments available to absorb light around a reaction center, and the reoxidation rate of the Quinone A in PSII ( $1/\tau$ ) (Kolber et al., 1994). Compared with P1706-C1,  $1/\tau$  increased in our C2 measurements. This response was not expected as rates of electron transport usually decrease under Fe limitation. However, Fe limitation during P1706-C2, was independently determined based on diagnostic nutrient ratios (Si:N and Fe:N; K. Fulton and K. Barbeau, personal communication, June 13, 2019) and Fe amendment experiments (K. Forsch and K. Barbeau, personal communication, February 13, 2020). Consequently,  $1/\tau$  was likely driven by changes in the phytoplankton community. The enhanced NPQ rates (Figure S2) demonstrated an enhanced energy dissipation through nonphotochemical processes in Fe-limited communities. This enhanced NPQ<sub>NSV</sub> did affect our productivity rate estimate, as NPQ<sub>NSV</sub> values are used to calculate the electron to carbon ratio (see eq. 7; Schuback et al., 2018). Data on photophysiology will not be discussed further, yet we decided to include those data here and in the Supporting Information as those data sets can inform the reader on underlying processes of productivity changes and limitations thereof.

## 5.2. Net Community, NP, and Export Flux

Nitrate consumed by phytoplankton often represents NP in the surface ocean and hence should equate to the amount of organic matter available for export (Eppley & Peterson, 1979), although it may be an overestimate if substantial nitrification occurs within the euphotic zone (Yool et al., 2007). Similarly, NCP represents the balance between organic matter production (photosynthesis) and organic matter consumption (respiration); hence, it should also approximate export when the organic pools are at steady state (Hamme et al., 2012; Li & Cassar, 2017). Crucially, we only expect a quantitative correspondence between NP, NCP, and export when integrating over sufficiently long temporal and large spatial scales (Plattner et al., 2005) and including all forms of exported organic matter (Boyd et al., 2019; Ducklow et al., 2001). Thus, comparisons of these kinds of measurements for short term in-situ or shipboard incubations in spatially heterogeneous regions like the CCE can be challenging to interpret.

Until recently, O<sub>2</sub>:Ar-based NCP estimates were only used in near-steady-state systems, assuming that time frames for NCP measurements (weeks to months) need to integrate all past changes in production, grazing, and physical disturbances. More recently, Teeter et al. (2018) showed that a strict steady-state assumption for NCP analysis is not required and that reliable rates of NCP can be obtained even if the community varies. This is because the NCP estimate is a weighted analysis of the current oxygen inventory combined with prior gas fluxes for which most weight is placed on the recent past. The weighting reduces historical influence and enhances more recent events. However, the uncertainty of the NCP estimate increases with the physical complexity of a region (Teeter et al., 2018). Due to the complex physical and biochemical nature of the CCE ecosystem, large discrepancies were expected in our method comparison. For example, although upwelling is typically associated with high primary production, the low oxygen content of freshly upwelled waters could be interpreted as negative NCP. On the other hand, upwelled water with accumulated biomass and high oxygen from the primary production would appear to be strongly net autotrophic, even if NCP had switched to negative. Despite these potential issues, the EIMS method has been usefully applied in other complex coastal environments, such as the Western Antarctic Peninsula (Eveleth et al., 2017; Tortell et al., 2014). Since we applied the EIMS method with a Lagrangian study, we are also able to measure changes in the O<sub>2</sub>/Ar ratio with high temporal resolution and resolve some of the uncertainties in measured signal versus true activity (Teeter et al., 2018; Wang et al., 2020).

Using the calculation of NCP<sub>inst</sub>, NCP production estimates should match the combined effects of NP and short-term changes in organic matter inventories. Our direct comparison reveals large mismatches, however (Figure 5, Tables 1 and S4). Four factors play an important role here: (1) NP estimates can never be negative while NCP can be negative, especially in a high-biomass system when grazing exceeds production over the time frame of measurements; (2) vertical advection or diffusion across isopycnals can introduce low-oxygen water into surface layers; (3) NCP rates are influenced by all organisms in the mixed layer, some of which undergo diurnal vertical migration and therefore introduce a vertical transport component to the mass

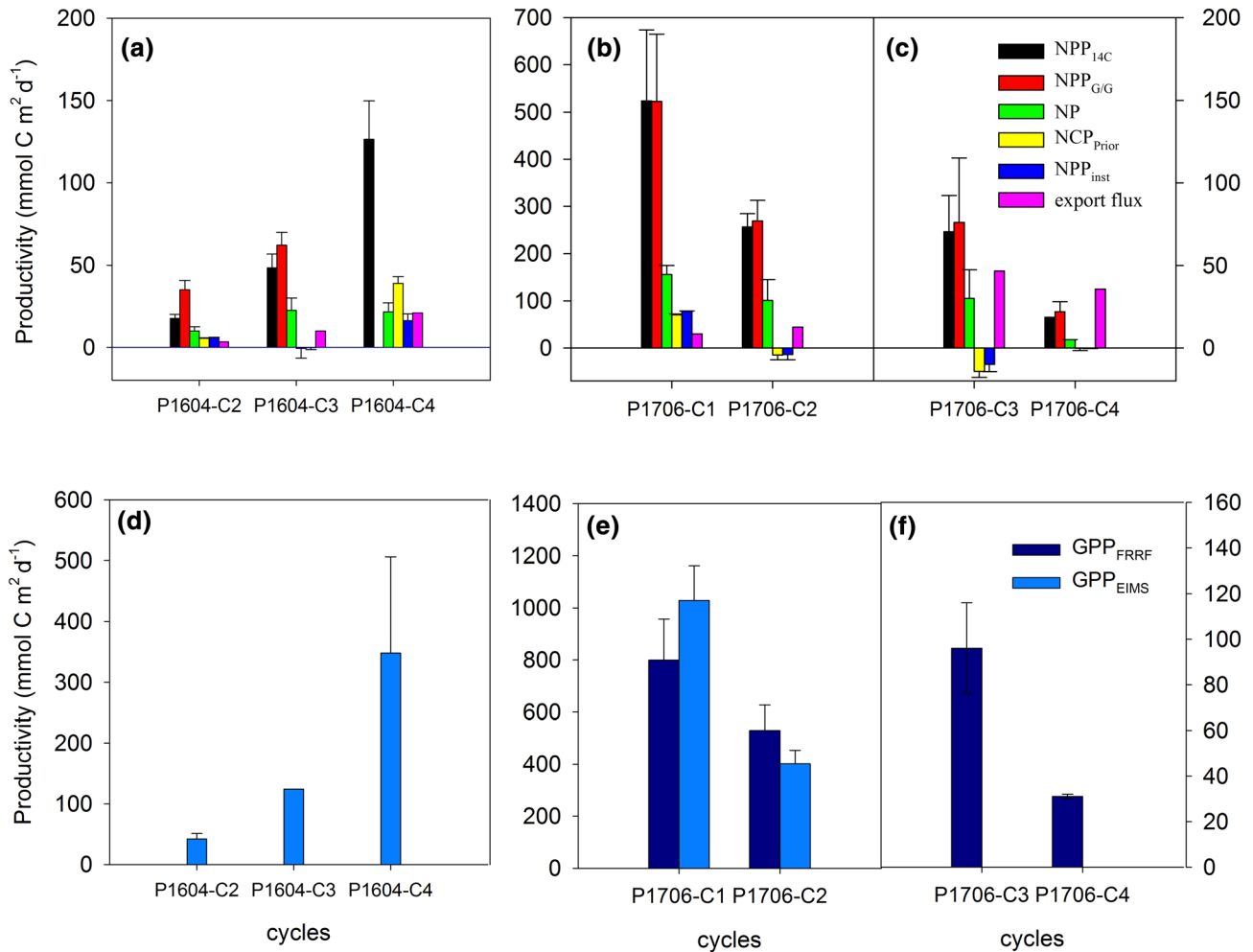


**Figure 5.** Summary of all production estimates. Data are normalized to carbon units. Note difference in scales between the graph panels.

balance; and (4) our Lagrangian approach was partially affected by ship movements during net tows and instrument recovery which introduce a non-Lagrangian error into NCP measurements.

As presented in section 4, our data show substantial discrepancies between NCP and NP. During P1604-C2 and C4, when regions of high variability were intentionally avoided, there was reasonable agreement, despite statistical differences, between NCP<sub>RT</sub> and NP measurements (NCP<sub>inst</sub> =  $6.0 \pm 0.1$  and NP =  $10.6 \pm 2.7$   $\text{mmol C m}^{-2} \text{d}^{-1}$  for P1604-C2; NCP<sub>inst</sub> =  $16.4 \pm 4.0$  and NP =  $23.2 \pm 5.9$   $\text{mmol C m}^{-2} \text{d}^{-1}$  for P1604-C4). For P1604-C3, however, NP was relatively high and positive ( $23.8 \pm 8$   $\text{mmol C m}^{-2} \text{d}^{-1}$ ) while NCP<sub>inst</sub> was negative ( $-0.1 \pm 1.1$   $\text{mmol C m}^{-2} \text{d}^{-1}$ ). On this cycle, surface Chl ( $1.0 \mu\text{g L}^{-1}$ ), surface  $\text{NO}_3^-$  ( $3.8 \mu\text{mol L}^{-1}$ ), and surface POC ( $7.1 \mu\text{mol C L}^{-1}$ ) were all high, but a dense swarm of doliolids, with high grazing and presumably high respiration, dominated the zooplankton (Morrow et al., 2018). It is thus likely that the discrepancy in P1604-C3 measurements was due to circumstances in which NCP and NP were temporarily decoupled, with nitrate fueling substantial NP even as high mesozooplankton grazing and respiration drove NCP towards net heterotrophy.

For P1706, the differences between NCP and NP were more pronounced. NP was reasonably high on all cycles, with mean  $f$  ratios varying from 0.27 to 0.49. NCP<sub>inst</sub> was high on P1706-C1 (although still only 49% of NP), but negative or near zero on all other cycles. These results might be explained by the unusual physical and biological dynamics of the mesoscale filament that was studied on this cruise. Specifically, the cruise targeted non-steady-state water parcels ranging from coastal upwelling on C1 to aged filament water mixed with offshore California Current water on C3, as well as water parcels during early and late



stages of a filament evolution (P1706-C2 and C4). Along this continuum from upwelling to offshore mixing, surface POC declined substantially from 38.5 to 5.7  $\mu\text{mol C L}^{-1}$  for P1706-C1 to C4. This biomass decline (during offshore transit over 2–3 weeks) would have to be matched by a combination of export and/or negative NCP along the transect. However, NP cannot be negative, and although  $\text{NO}_3^-$  decreased from inshore to offshore, surface nitrate remained relatively high (2.9  $\mu\text{mol C L}^{-1}$ ), allowing continued NP. Ammonium also accumulated between P1706-C1 and P1706-C4 (from 0.4 to 1.8  $\mu\text{mol L}^{-1}$ ), as would be expected if remineralization exceeded phytoplankton production. Our results are thus consistent with a system in which NCP peaked early in the bloom and switched to negative as the bloom declined. A similar NP and NCP pattern was observed following a coastal Antarctic bloom (Stukel et al., 2015b; Tortell et al., 2014). The NCP estimates could have also been affected by upwelling and/or vertical diffusion in this energetic mesoscale environment, which would underestimate NCP if low- $\text{O}_2$  water was introduced from below the mixed layer (Wang et al., 2020 for potential impact on NCP). In addition, nitrate uptake could overestimate NP if substantial nitrification occurs in the euphotic zone. This would seem an unlikely scenario, given the estimates of mixed-layer nitrification in the CCE (4.6  $\text{nmol L}^{-1} \text{d}^{-1}$ ; Santoro et al., 2013) that are relatively low compared with nitrate uptake rates. However, nitrification might be more active in filaments.

Ultimately, NP and NCP should be balanced by export production. Our results show, however, that export flux was substantially lower than NP across the region (Figure 5). When integrated to the base of the euphotic zone (data not shown) to match sediment trap data, NP exceeded export for all three cycles of P1604 and for all cycles of P1706 except C4 (at the end of the filament). For all the cycles of P1706, NP averaged 2.7 times higher than sinking flux. The same pattern did not hold for NCP in P1706 because of multiple cycles with negative NCP. In a non-steady-state system, however, export should be balanced not by NCP alone, but by the sum of NCP and POC decline, unless large parts of NCP are also going into DOC buildup. Because P1706-C4 was a transport extension of C2, we can test this balance over the 12 days that separate the beginning and end of those cycles. Over this period, POC declined from 1,078 to 510  $\text{mmol C m}^{-2}$ , equating to a decline of 43.6  $\text{mmol C m}^{-2} \text{d}^{-1}$ . This is remarkably equal to the mean export during these two cycles (40.1  $\text{mmol C m}^{-2} \text{d}^{-1}$ ), suggesting that the declining biomass would have been sufficient to support all the measured export flux even if no additional biomass was produced.

The measurement of NP in excess of sinking flux is not a novel result. Nitrate uptake has also been reported to exceed the sinking particle export in the Western Antarctic Peninsula (Ducklow et al., 2018; Stukel et al., 2015a), the Bermuda Atlantic Time Series site (Lipschultz, 2001; Lomas et al., 2013), the Arabian Sea (Buesseler et al., 1998; Sambrotto, 2001), and the Costa Rica Dome (Stukel et al., 2016). In addition, NCP has been found to exceed sinking flux in the Sargasso Sea (Estapa et al., 2015) and the Western Antarctic Peninsula (Stukel et al., 2015a). Within the CCE, prior studies have determined  $e$  ratios of  $\sim 0.2$  (Kelly et al., 2018), compared with  $f$  ratios frequently  $> 0.5$  (Harrison et al., 1987) and a region-wide NCP/NPP ratio of 0.4 (Munro et al., 2013). This deficiency of sinking export relative to NP and NCP likely reflects the importance of nonsinking forms of export including active transport of carbon by diel vertical migrants (Bianchi et al., 2013; Steinberg et al., 2000) and subduction of particulate and dissolved organic matter (Carlson et al., 1994; Omand et al., 2015). Within the CCE, subduction of particles has been shown to be a substantial flux of organic matter out of the euphotic zone, although subducted particles did not penetrate deep into the ocean interior (Stukel et al., 2018). Active transport has also been shown to be substantial, and even to rival sinking flux, in high-biomass regions of the CCE (Kelly et al., 2019). Together, these other processes likely explain our measurement discrepancies between NP and export.

## 6. Conclusions

Our study presents a well-constrained characterization of GPP, NPP, NCP, NP, and export production in a complex and heterogeneous physical environment. The results show how a multimethod approach can clarify some of the variabilities and inconsistencies observed using different methods. We found strong spatial gradients in productivity rates from coastal to offshore regions that were primarily driven by decreasing biomass and nutrient availability with distance from shore, and we showed that the high-resolution measurements applied here resolved diel patterns in GPP and NCP. Overall, all our data from temporally resolved production estimates are surprisingly consistent, within the errors of the estimates, with data from traditional 24-h production measurements. The GPP:NPP ratio was approximately 2 over the study region,

with no distinct spatial pattern. The  $f$  ratios (NP:NPP) varied from 0.16 to 0.55, suggesting that recycled  $\text{NH}_4^+$  was typically the most important nutrient supporting production, even though nitrate was still a major source of N. NP typically exceeded carbon export of sinking particles by a large margin, suggesting that temporally and spatially decoupled export (vertical migration of grazers, water mass subduction) must be quantitatively important for resolving the region's carbon budget. Since underway high temporal resolution analyses of productivity using FRRF and EIMS match general ecosystem expectations, we suggest that temporally resolved production methods should be employed regularly to enhance understanding of physically complex and economically important ecosystems.

#### Acknowledgments

The authors declare no conflict of interest. Data sets for this research can be accessed at the CCE-LTER Datazoo online database (<https://oceaninformatics.ucsd.edu/datazoo/catalogs/ccelter/datasets>). This study was funded by US National Science Foundation grants OCE-1637632 (CCE-LTER) and OCE-1614359 (RAPID). We appreciate the contributions to shipboard sampling and analyses by Ali Freibott, Belli Valencia, Shonna Dovel and Megan Roadman and Cameron Quackenbush. We also want to thank the captains and the crews of the *R/V Sikuliaq* and *R/V Roger Revelle* for their support. We appreciated the help during both cruises by chief scientist Mark Ohman. We also want to thank Kathy Barbeau and Kiefer Forsch for their discussion of their preliminary data on iron limitation during these cruises.

#### References

- Barron, R. K., Siegel, D. A., & Guillocheau, N. (2014). Evaluating the importance of phytoplankton community structure to the optical properties of the Santa Barbara Channel, California. *Limnology and Oceanography*, *59*(3), 927–946. <https://doi.org/10.4319/lo.2014.59.3.0927>
- Behrenfeld, M. J., & Falkowski, P. G. (1997). Photosynthetic rates derived from satellite-based chlorophyll concentration. *Limnology and Oceanography*, *42*(1), 1–20. <https://doi.org/10.4319/lo.1997.42.1.0001>
- Bercl, T. L., & Kranz, S. A. (2019). Insights into carbon acquisition and photosynthesis in *Karenia brevis* under a range of CO<sub>2</sub> concentrations. *Progress in Oceanography*, *172*, 65–76. <https://doi.org/10.1016/j.pocean.2019.01.011>
- Bianchi, D., Stock, C., Galbraith, E. D., & Sarmiento, J. L. (2013). Diel vertical migration: Ecological controls and impacts on the biological pump in a one-dimensional ocean model. *Global Biogeochemical Cycles*, *27*(2), 478–491. <https://doi.org/10.1002/gbc.20031>
- Boatman, T. G., Geider, R. J., & Oxborough, K. (2019). Improving the accuracy of single turnover active fluorometry (STAF) for the estimation of phytoplankton primary productivity (PhytoPP). *bioRxiv*, 6(319), 583591.
- Bond, N. A., Cronin, M. F., Freeland, H., & Mantua, N. (2015). Causes and impacts of the 2014 warm anomaly in the NE Pacific. *Geophysical Research Letters*, *42*(9), 3414–3420. <https://doi.org/10.1002/2015GL063306>
- Boyd, P. W., Claustre, H., Levy, M., Siegel, D. A., & Weber, T. (2019). Multi-faceted particle pumps drive carbon sequestration in the ocean. *Nature*, *568*(7752), 327–335. <https://doi.org/10.1038/s41586-019-1098-2>
- Bronk, D. A., Glibert, P. M., & Ward, B. B. (1994). Nitrogen uptake, dissolved organic nitrogen release, and new production. *Science*, *265*(5180), 1843–1846. <https://doi.org/10.1126/science.265.5180.1843>
- Buesseler, K., Ball, L., Andrews, J., Benitez-Nelson, C., Belastock, R., Chai, F., & Chao, Y. (1998). Upper ocean export of particulate organic carbon in the Arabian Sea derived from thorium-234. *Deep Sea Research, Part II*, *45*(10–11), 2461–2487. [https://doi.org/10.1016/S0967-0645\(98\)80022-2](https://doi.org/10.1016/S0967-0645(98)80022-2)
- Carlson, C. A., Ducklow, H. W., & Michaels, A. F. (1994). Annual flux of dissolved organic-carbon from the euphotic zone in the north-western Sargasso Sea. *Nature*, *371*(6496), 405–408. <https://doi.org/10.1038/371405a0>
- Cassar, N., Barnett, B. A., Bender, M. L., Kaiser, J., Hamme, R. C., & Tilbrook, B. (2009). Continuous high-frequency dissolved O<sub>2</sub>/Ar measurements by equilibrator inlet mass spectrometry. *Analytical Chemistry*, *81*(5), 1855–1864. <https://doi.org/10.1021/ac802300u>
- Chavez, F. P., & Messie, M. (2009). A comparison of eastern boundary upwelling ecosystems. *Progress in Oceanography*, *83*(1–4), 80–96. <https://doi.org/10.1016/j.pocean.2009.07.032>
- Collos, Y. (1998). Nitrate uptake, nitrite release and uptake, and new production estimates. *Marine Ecology Progress Series*, *171*, 293–301. <https://doi.org/10.3354/meps171293>
- Ducklow, H. W., Steinberg, D. K., & Buesseler, K. O. (2001). Upper ocean carbon export and the biological pump. *Oceanography* *14*(4), 0–58, 50. <https://doi.org/10.5670/oceanog.2001.06>
- Ducklow, H. W., Stukel, M. R., Eveleth, R., Doney, S. C., Jickells, T., Schofield, O., et al. (2018). Spring-summer net community production, new production, particle export and related water column biogeochemical processes in the marginal sea ice zone of the Western Antarctic Peninsula 2012–2014. *Philosophical Transactions of the Royal Society a-Mathematical Physical and Engineering Sciences*, *376*(2122), 20170177. <https://doi.org/10.1098/rsta.2017.0177>
- Dugdale, R. C. (1972). Chemical oceanography and primary productivity in upwelling regions. *Geoforum*, *3*(3), 47–61. [https://doi.org/10.1016/0016-7185\(72\)90085-1](https://doi.org/10.1016/0016-7185(72)90085-1)
- Dugdale, R. C., & Goering, J. J. (1967). Uptake of new and regenerated forms of nitrogen in primary productivity. *Limnology and Oceanography*, *12*(2), 196–206. <https://doi.org/10.4319/lo.1967.12.2.0196>
- Dugdale, R. C., & Wilkerson, F. P. (1986). The use of <sup>15</sup>N to measure nitrogen uptake in eutrophic oceans—Experimental considerations. *Limnology and Oceanography*, *31*(4), 673–689. <https://doi.org/10.4319/lo.1986.31.4.0673>
- Dunne, J. P., Sarmiento, J. L., & Gnanadesikan, A. (2007). A synthesis of global particle export from the surface ocean and cycling through the ocean interior and on the seafloor. *Global Biogeochemical Cycles*, *21*(4), .<https://doi.org/10.1029/2006GB002907>
- Eppley, R. W., & Peterson, B. J. (1979). Particulate organic-matter flux and planktonic new production in the deep ocean. *Nature*, *282*(5740), 677–680. <https://doi.org/10.1038/282677a0>
- Estapa, M. L., Siegel, D. A., Buesseler, K. O., Stanley, R. H. R., Lomas, M. W., & Nelson, N. B. (2015). Decoupling of net community and export production on submesoscales. *Global Biogeochemical Cycles*, *29*(8), 1266–1282. <https://doi.org/10.1002/2014GB004913>
- Eveleth, R., Cassar, N., Doney, S. C., Munro, D. R., & Sweeney, C. (2017). Biological and physical controls on O<sub>2</sub>/Ar, Ar and pCO<sub>2</sub> variability at the Western Antarctic Peninsula and in the Drake Passage. *Deep Sea Research, Part II*, *139*, 77–88. <https://doi.org/10.1016/j.dsr2.2016.05.002>
- Falkowski, P. G., & Kolber, Z. (1993). Estimation of phytoplankton photosynthesis by active fluorescence. Paper presented at the Measurement of Primary Production from the Molecular to the Global Scale.
- Goldman, J. A. L., Kranz, S. A., Young, J. N., Tortell, P. D., Stanley, R. H. R., Bender, M. L., & Morel, F. M. M. (2015). Gross and net production during the spring bloom along the Western Antarctic Peninsula. *New Phytologist*, *205*(1), 182–191. <https://doi.org/10.1111/nph.13125>
- Gordon, L. I., Jennings, J. C., Ross, A. A., & Krest, J. M. (1992). A suggested Protocol for Continuous Flow Automated Analysis of Seawater Nutrients in the WOCE Hydrographic Program and the Joint Global Ocean Fluxes Study Grp. *Tech Rpt OSU College of Oceanography Descrip. Chem Oc.*, *92*(1), 29–39.

- Hamme, R. C., Cassar, N., Lance, V. P., Vaillancourt, R. D., Bender, M. L., Strutton, P. G., et al. (2012). Dissolved O<sub>2</sub>/Ar and other methods reveal rapid changes in productivity during a Lagrangian experiment in the Southern Ocean. *Journal of Geophysical Research*, 117. <https://doi.org/10.1029/2011JC007046>
- Harrison, W. G., Platt, T., & Lewis, M. R. (1987). F-ratio and its relationship to ambient nitrate concentration in coastal waters. *Journal of Plankton Research*, 9(1), 235–248. <https://doi.org/10.1093/plankt/9.1.235>
- Hashimoto, S., Horimoto, N., Yamaguchi, Y., Ishimaru, T., & Saino, T. (2005). Relationship between net and gross primary production in the Sagami Bay, Japan. *Limnology and Oceanography*, 50(6), 1830–1835. <https://doi.org/10.4319/lo.2005.50.6.1830>
- Iriarte, A. (1999). The influence of irradiance on the apparent photosynthetic quotient in the unicellular alga *Pycnococcus provasolii*. *Cahiers de Biologie Marine*, 40(1), 29–33.
- Jacox, M. G., Hazen, E. L., Zaba, K. D., Rudnick, D. L., Edwards, C. A., Moore, A. M., & Bograd, S. J. (2016). Impacts of the 2015–2016 El Niño on the California Current System: Early assessment and comparison to past events. *Geophysical Research Letters*, 43, 7072–7080. <https://doi.org/10.1002/2016GL069716>
- Kahru, M., Jacox, M. G., Lee, Z., Kudela, R. M., Manzano-Sarabia, M., & Mitchell, B. G. (2015). Optimized multi-satellite merger of primary production estimates in the California Current using inherent optical properties. *Journal of Marine Systems*, 147, 94–102. <https://doi.org/10.1016/j.jmarsys.2014.06.003>
- Kanda, J., Itoh, T., Ishikawa, D., & Watanabe, Y. (2003). Environmental control of nitrate uptake in the East China Sea. *Deep Sea Research, Part II*, 50(2), 403–422. [https://doi.org/10.1016/S0967-0645\(02\)00464-2](https://doi.org/10.1016/S0967-0645(02)00464-2)
- Kelly, T. B., Davison, P. C., Goericke, R., Landry, M. R., Ohman, M. D., & Stukel, M. R. (2019). The Importance of mesozooplankton diel vertical migration for sustaining a mesopelagic food Web. *bioRxiv*, 642(975).
- Kelly, T. B., Goericke, R., Kahru, M., Song, H., & Stukel, M. R. (2018). CCE II: Spatial and interannual variability in export efficiency and the biological pump in an eastern boundary current upwelling system with substantial lateral advection. *Deep Sea Research, Part I*, 140, 14–25. <https://doi.org/10.1016/j.dsr.2018.08.007>
- Knauer, G. A., Martin, J. H., & Bruland, K. W. (1979). Fluxes of particulate carbon, nitrogen, and phosphorus in the upper water column of the Northeast Pacific. *Deep Sea Research, Part I*, 26(1), 97–108. [https://doi.org/10.1016/0198-0149\(79\)90089-X](https://doi.org/10.1016/0198-0149(79)90089-X)
- Kolber, Z., & Falkowski, P. G. (1993). Use of active fluorescence to estimate phytoplankton photosynthesis in-situ. *Limnology and Oceanography*, 38(8), 1646–1665. <https://doi.org/10.4319/lo.1993.38.8.1646>
- Kolber, Z. S., Barber, R. T., Coale, K. H., Fitzwater, S. E., Greene, R. M., Johnson, K. S., et al. (1994). Iron limitation of phytoplankton photosynthesis in the equatorial Pacific-Ocean. *Nature*, 371(6493), 145–149. <https://doi.org/10.1038/371145a0>
- Kranz, S. A., Levitan, O., Richter, K.-U., Prasil, O., Berman-Frank, I., & Rost, B. (2010). Combined effects of CO<sub>2</sub> and light on the N<sub>2</sub>-fixing cyanobacterium *Trichodesmium* IMS101: Physiological responses. *Plant Physiology*, 154(1), 334–345. <https://doi.org/10.1104/pp.110.159145>
- Kudela, R. M., Banas, N. S., Barth, J. A., Frame, E. R., Jay, D. A., Largier, J. L., et al. (2008). New insights into the controls and mechanisms of plankton productivity in coastal upwelling waters of the Northern California Current System. *Oceanography*, 21(4), 46–59. <https://doi.org/10.5670/oceanog.2008.04>
- Kumar, N., Anderson, R. F., Mortlock, R. A., Froelich, P. N., Kubik, P., Ditttrichhannen, B., & Suter, M. (1995). Increased biological productivity and export production in the glacial Southern-Ocean. *Nature*, 378(6558), 675–680. <https://doi.org/10.1038/378675a0>
- Landry, M. R., Brown, S. L., Rii, Y. M., Selph, K. E., Bidigare, R. R., Yang, E. J., & Simmons, M. P. (2008). Depth-stratified phytoplankton dynamics in Cyclone Opal, a subtropical mesoscale eddy. *Deep Sea Research, Part II*, 55(10–13), 1348–1359. <https://doi.org/10.1016/j.dsr2.2008.02.001>
- Landry, M. R., Constantinou, J., Latasa, M., Brown, S. L., Bidigare, R. R., & Ondrusek, M. E. (2000). Biological response to iron fertilization in the eastern equatorial Pacific (IronEx II). III. Dynamics of phytoplankton growth and microzooplankton grazing. *Marine Ecology Progress Series*, 201, 57–72. <https://doi.org/10.3354/meps201057>
- Landry, M. R., & Hassett, R. P. (1982). Estimating the grazing impact of marine micro-zooplankton. *Marine Biology*, 67(3), 283–288. <https://doi.org/10.1007/BF00397668>
- Landry, M. R., Ohman, M. D., Goericke, R., Stukel, M. R., Barbeau, K. A., Bundy, R., & Kahru, M. (2012). Pelagic community responses to a deep-water front in the California Current Ecosystem: Overview of the A-Front Study. *Journal of Plankton Research*, 34(9), 739–748. <https://doi.org/10.1093/plankt/fbs025>
- Landry, M. R., Selph, K. E., Decima, M., Gutierrez-Rodriguez, A., Stukel, M. R., Taylor, A. G., & Pasulka, A. L. (2016). Phytoplankton production and grazing balances in the Costa Rica Dome. *Journal of Plankton Research*, 38(2), 366–379. <https://doi.org/10.1093/plankt/fbv089>
- Landry, M. R., Selph, K. E., Taylor, A. G., Decima, M., Balch, W. M., & Bidigare, R. R. (2011). Phytoplankton growth, grazing and production balances in the HNLC equatorial Pacific. *Deep Sea Research, Part II*, 58(3–4), 524–535. <https://doi.org/10.1016/j.dsr2.2010.08.011>
- Landry, M. R., Selph, K. E., & Yang, E. J. (2011). Decoupled phytoplankton growth and microzooplankton grazing in the deep euphotic zone of the eastern equatorial Pacific. *Marine Ecology Progress Series*, 421, 13–24. <https://doi.org/10.3354/meps08792>
- Lawrenz, E., Silsbe, G., Capuzzo, E., Ylostalo, P., Forster, R. M., Simis, S. G. H., et al. (2013). Predicting the electron requirement for carbon fixation in seas and oceans. *PLoS ONE*, 8(3), e58137. <https://doi.org/10.1371/journal.pone.0058137>
- Laws, E. A., Landry, M. R., Barber, R. T., Campbell, L., Dickson, M. L., & Marra, J. (2000). Carbon cycling in primary production bottle incubations: Inferences from grazing experiments and photosynthetic studies using (14)C and (18)O in the Arabian Sea. *Deep Sea Research, Part II*, 47(7–8), 1339–1352. [https://doi.org/10.1016/S0967-0645\(99\)00146-0](https://doi.org/10.1016/S0967-0645(99)00146-0)
- Li, Q. P., Franks, P. J. S., Landry, M. R., Goericke, R., & Taylor, A. G. (2010). Modeling phytoplankton growth rates and chlorophyll to carbon ratios in California coastal and pelagic ecosystems. *Journal of Geophysical Research – Biogeosciences*, 115(G4), G04003. <https://doi.org/10.1029/2009JG001111>
- Li, Z. C., & Cassar, N. (2017). A mechanistic model of an upper bound on oceanic carbon export as a function of mixed layer depth and temperature. *Biogeosciences*, 14(22), 5015–5027. <https://doi.org/10.5194/bg-14-5015-2017>
- Lipschultz, F. (2001). A time-series assessment of the nitrogen cycle at BATS. *Deep Sea Research, Part II*, 48(8–9), 1897–1924. [https://doi.org/10.1016/S0967-0645\(00\)00168-5](https://doi.org/10.1016/S0967-0645(00)00168-5)
- Lomas, M. W., Bates, N. R., Johnson, R. J., Knap, A. H., Steinberg, D. K., & Carlson, C. A. (2013). Two decades and counting: 24-years of sustained open ocean biogeochemical measurements in the Sargasso Sea. *Deep Sea Research, Part II*, 93, 16–32. <https://doi.org/10.1016/j.dsr2.2013.01.008>
- Longhurst, A., Sathyendranath, S., Platt, T., & Caverhill, C. (1995). An estimate of global primary production in the ocean from satellite radiometer data. *Journal of Plankton Research*, 17(6), 1245–1271. <https://doi.org/10.1093/plankt/17.6.1245>

- López-Sandoval, D. C., Rodríguez-Ramos, T., Cermeño, P., Sobrino, C., & Marañón, E. (2014). Photosynthesis and respiration in marine phytoplankton: Relationship with cell size, taxonomic affiliation, and growth phase. *Journal of Experimental Marine Biology and Ecology*, 457, 151–159. <https://doi.org/10.1016/j.jembe.2014.04.013>
- Luz, B., & Barkan, E. (2005). The isotopic ratios  $^{17}\text{O}/^{16}\text{O}$  and  $^{18}\text{O}/^{16}\text{O}$  in molecular oxygen and their significance in biogeochemistry. *Geochimica et Cosmochimica Acta*, 69(5), 1099–1110. <https://doi.org/10.1016/j.gca.2004.09.001>
- Marra, J. (2009). Net and gross productivity: Weighing in with  $^{14}\text{C}$ . *Aquatic Microbial Ecology*, 56(2), 123–131. <https://doi.org/10.3354/ame01306>
- Michaels, A. F., & Silver, M. W. (1988). Primary production, sinking fluxes and the microbial food web. *Deep Sea Research, Part I*, 35(4), 473–490. [https://doi.org/10.1016/0198-0149\(88\)90126-4](https://doi.org/10.1016/0198-0149(88)90126-4)
- Moore, C. M., Suggett, D. J., Hickman, A. E., Kim, Y. N., Tweddle, J. F., Sharples, J., et al. (2006). Phytoplankton photoacclimation and photoadaptation in response to environmental gradients in a shelf sea. *Limnology and Oceanography*, 51(2), 936–949. <https://doi.org/10.4319/lom.2006.51.2.0936>
- Morrow, R. M., Ohman, M. D., Goericke, R., Kelly, T. B., Stephens, B. M., & Stukel, M. R. (2018). CCE V: Primary production, mesozooplankton grazing, and the biological pump in the California Current Ecosystem: Variability and response to El Niño. *Deep Sea Research, Part I*, 140, 52–62. <https://doi.org/10.1016/j.dsr.2018.07.012>
- Muller-Karger, F. E., Varela, R., Thunell, R., Luerssen, R., Hu, C. M., & Walsh, J. J. (2005). The importance of continental margins in the global carbon cycle. *Geophysical Research Letters*, 32, L01602. <https://doi.org/10.1029/2004GL021346>
- Munro, D. R., Quay, P. D., Juraneck, L. W., & Goericke, R. (2013). Biological production rates off the Southern California coast estimated from triple  $\text{O}_2$  isotopes and  $\text{O}_2$ : Ar gas ratios. *Limnology and Oceanography*, 58(4), 1312–1328. <https://doi.org/10.4319/lom.2013.58.4.1312>
- Myklestad, S. M. (2000). Dissolved organic carbon from phytoplankton. In P. Wangersky (Ed). *The handbook of environmental chemistry [D], Marine chemistry* (pp. 111–148). Switzerland: Springer, Berlin.
- Nagai, T., Gruber, N., Frenzel, H., Lachkar, Z., McWilliams, J. C., & Plattner, G. K. (2015). Dominant role of eddies and filaments in the offshore transport of carbon and nutrients in the California Current System. *Journal of Geophysical Research*, 120(8), 5318–5341. <https://doi.org/10.1002/2015JC010889>
- Nickels, C. F., & Ohman, M. D. (2018). CCEIII: Persistent functional relationships between copepod egg production rates and food concentration through anomalously warm conditions in the California current ecosystem. *Deep Sea Research, Part I*, 140, 26–35. <https://doi.org/10.1016/j.dsr.2018.07.001>
- Ohman, M. D., Powell, J. R., Picheral, M., & Jensen, D. W. (2012). Mesozooplankton and particulate matter responses to a deep-water frontal system in the southern California Current System. *Journal of Plankton Research*, 34(9), 815–827. <https://doi.org/10.1093/plankt/fbs028>
- Omand, M. M., D'Asaro, E. A., Lee, C. M., Perry, M. J., Briggs, N., Cetinic, I., & Mahadevan, A. (2015). Eddy-driven subduction exports particulate organic carbon from the spring bloom. *Science*, 348(6231), 222–225. <https://doi.org/10.1126/science.1260062>
- O'Reilly, J. E., Maritorena, S., Mitchell, B. G., Siegel, D. A., Carder, K. L., Garver, S. A., et al. (1998). Ocean color chlorophyll algorithms for SeaWiFS. *Journal of Geophysical Research-Oceans*, 103(C11), 24937–24953. <https://doi.org/10.1029/98JC02160>
- Oxborough, K., Moore, C. M., Suggett, D. J., Lawson, T., Chan, H. G., & Geider, R. J. (2012). Direct estimation of functional PSII reaction center concentration and PSII electron flux on a volume basis: A new approach to the analysis of fast repetition rate fluorometry (FRRF) data. *Limnology and Oceanography: Methods*, 10(3), 142–154. <https://doi.org/10.4319/lom.2012.10.142>
- Painter, S. C., Sanders, R., Poulton, A. J., Woodward, E. M. S., Lucas, M., & Chamberlain, K. (2007). Nitrate uptake at photic zone depths is not important for export in the subtropical ocean. *Global Biogeochemical Cycles*, 21(4). <https://doi.org/10.1029/2006GB002807>
- Pan, X. J., Mannino, A., Marshall, H. G., Filippino, K. C., & Mulholland, M. R. (2011). Remote sensing of phytoplankton community composition along the northeast coast of the United States. *Remote Sensing of Environment*, 115(12), 3731–3747. <https://doi.org/10.1016/j.rse.2011.09.011>
- Peterson, B. J. (1980). Aquatic primary productivity and the  $\text{C}_{14}$ - $\text{CO}_2$  method—A history of the productivity problem. *Annual Review of Ecology and Systematics*, 11(1), 359–385. <https://doi.org/10.1146/annurev.es.11.110180.002043>
- Platt, T., Gallegos, C. L., & Harrison, W. G. (1980). Photoinhibition of photosynthesis in natural assemblages of marine-phytoplankton. *Journal of Marine Research*, 38(4), 687–701.
- Plattner, G. K., Gruber, N., Frenzel, H., & McWilliams, J. C. (2005). Decoupling marine export production from new production. *Geophysical Research Letters*, 32(11), L11612. <https://doi.org/10.1029/2005GL022660>
- Quay, P. D., Peacock, C., Bjorkman, K., & Karl, D. M. (2010). Measuring primary production rates in the ocean: Enigmatic results between incubation and non-incubation methods at Station ALOHA. *Global Biogeochemical Cycles*, 24(3). <https://doi.org/10.1029/2009GB003665>
- Reuer, M. K., Barnett, B. A., Bender, M. L., Falkowski, P. G., & Hendricks, M. B. (2007). New estimates of Southern Ocean biological production rates from O-2/Ar ratios and the triple isotope composition of O-2. *Deep Sea Research, Part I*, 54(6), 951–974. <https://doi.org/10.1016/j.dsr.2007.02.007>
- Robinson, C., Tilstone, G. H., Rees, A. P., Smyth, T. J., Fishwick, J. R., Tarran, G. A., et al. (2009). Comparison of in vitro and in situ plankton production determinations. *Aquatic Microbial Ecology*, 54(1), 13–34. <https://doi.org/10.3354/ame01250>
- Saba, V. S., Friedrichs, M. A. M., Antoine, D., Armstrong, R. A., Asanuma, I., Behrenfeld, M. J., et al. (2011). An evaluation of ocean color model estimates of marine primary productivity in coastal and pelagic regions across the globe. *Biogeosciences*, 8(2), 489–503. <https://doi.org/10.5194/bg-8-489-2011>
- Sambrotto, R. N. (2001). Nitrogen production in the northern Arabian Sea during the spring intermonsoon and southwest monsoon seasons. *Deep Sea Research, Part II*, 48(6–7), 1173–1198. [https://doi.org/10.1016/S0967-0645\(00\)00135-1](https://doi.org/10.1016/S0967-0645(00)00135-1)
- Santorio, A. E., Sakamoto, C. M., Smith, J. M., Plant, J. N., Gehman, A. L., Worden, A. Z., et al. (2013). Measurements of nitrite production in and around the primary nitrite maximum in the central California Current. *Biogeosciences*, 10(11), 7395–7410. <https://doi.org/10.5194/bg-10-7395-2013>
- Schuback, N., Hoppe, C. J. M., Tremblay, J. E., Maldonado, M. T., & Tortell, P. D. (2018). Primary productivity and the coupling of photosynthetic electron transport and carbon fixation in the Arctic Ocean (vol 62, pg 898, 2017). *Limnology and Oceanography*, 63(3), 1444–1444.
- Schuback, N., & Tortell, P. D. (2019). Diurnal regulation of photosynthetic light absorption, electron transport and carbon fixation in two contrasting oceanic environments. *Biogeosciences*, 16(7), 1381–1399. <https://doi.org/10.5194/bg-16-1381-2019>
- Spilling, K., Ylostalo, P., Simis, S., & Seppala, J. (2015). Interaction effects of light, temperature and nutrient limitations (N, P and Si) on growth, stoichiometry and photosynthetic parameters of the cold-water diatom *Chaetoceros wighamii*. *PLoS ONE*, 10(5), e0126308. <https://doi.org/10.1371/journal.pone.0126308>

- Stemann Nielsen, E. (1952). He use of radio-active carbon (C14) for measuring organic production in the sea. *ICES Journal of Marine Science*, 18(2), 117–140. <https://doi.org/10.1093/icesjms/18.2.117>
- Steinberg, D. K., Carlson, C. A., Bates, N. R., Goldthwait, S. A., Madin, L. P., & Michaels, A. F. (2000). Zooplankton vertical migration and the active transport of dissolved organic and inorganic carbon in the Sargasso Sea. *Deep Sea Research, Part I*, 47(1), 137–158. [https://doi.org/10.1016/S0967-0637\(99\)00052-7](https://doi.org/10.1016/S0967-0637(99)00052-7)
- Stock, C., & Dunne, J. (2010). Controls on the ratio of mesozooplankton production to primary production in marine ecosystems. *Deep Sea Research, Part I*, 57(1), 95–112. <https://doi.org/10.1016/j.dsr.2009.10.006>
- Strickland, J. D., & Parsons, T. R. (1972). A practical handbook of seawater analysis. In *Bulletin of the Fisheries Research Board of Canada* (2nd ed., Vol. 167, Part IV, pp. 185–193). Ottawa, Canada: Alger Press Ltd.
- Stukel, M. R., Asher, E., Couto, N., Schofield, O., Strelbel, S., Tortell, P., & Ducklow, H. W. (2015). The imbalance of new and export production in the western Antarctic Peninsula, a potentially “leaky” ecosystem. *Global Biogeochemical Cycles*, 29(9), 1400–1420. <https://doi.org/10.1002/2015GB005211>
- Stukel, M. R., Benitez-Nelson, C. R., Decima, M., Taylor, A. G., Buchwald, C., & Landry, M. R. (2016). The biological pump in the Costa Rica Dome: An open-ocean upwelling system with high new production and low export. *Journal of Plankton Research*, 38(2), 348–365. <https://doi.org/10.1093/plankt/fbv097>
- Stukel, M. R., Goericke, R., & Landry, M. R. (2019). Predicting primary production in the southern California Current Ecosystem from chlorophyll, nutrient concentrations, and irradiance. *bioRxiv*, 590240. <https://doi.org/10.1101/590240>
- Stukel, M. R., Kahru, M., Benitez-Nelson, C. R., Decima, M., Goericke, R., Landry, M. R., & Ohman, M. D. (2015). Using Lagrangian-based process studies to test satellite algorithms of vertical carbon flux in the eastern North Pacific Ocean. *Journal of Geophysical Research: Oceans*, 120, 7208–7222. <https://doi.org/10.1002/2015JC011264>
- Stukel, M. R., Kelly, T. B., Aluwihare, L. L., Barbeau, K. A., Goericke, R., Krause, J. W., et al. (2019). The carbon:(234)thorium ratios of sinking particles in the California Current Ecosystem 1: Relationships with plankton ecosystem dynamics. *Marine Chemistry*, 212, 1–15. <https://doi.org/10.1016/j.marchem.2019.01.003>
- Stukel, M. R., Landry, M. R., Ohman, M. D., Goericke, R., Samo, T., & Benitez-Nelson, C. R. (2012). Do inverse ecosystem models accurately reconstruct plankton trophic flows? Comparing two solution methods using field data from the California Current. *Journal of Marine Systems*, 91(1), 20–33. <https://doi.org/10.1016/j.jmarsys.2011.09.004>
- Stukel, M. R., Ohman, M. D., Benitez-Nelson, C. R., & Landry, M. R. (2013). Contributions of mesozooplankton to vertical carbon export in a coastal upwelling system. *Marine Ecology Progress Series*, 491, 47–65. <https://doi.org/10.3354/meps10453>
- Stukel, M. R., Song, H., Goericke, R., & Miller, A. J. (2018). The role of subduction and gravitational sinking in particle export, carbon sequestration, and the remineralization length scale in the California Current Ecosystem. *Limnology and Oceanography*, 63(1), 363–383. <https://doi.org/10.1002/lno.10636>
- Suggett, D., Kraay, G., Holligan, P., Davey, M., Aiken, J., & Geider, R. (2001). Assessment of photosynthesis in a spring cyanobacterial bloom by use of a fast repetition rate fluorometer. *Limnology and Oceanography*, 46(4), 802–810. <https://doi.org/10.4319/lo.2001.46.4.0802>
- Teeter, L., Hamme, R. C., Ianson, D., & Bianucci, L. (2018). Accurate estimation of net community production from O-2/Ar measurements. *Global Biogeochemical Cycles*, 32(8), 1163–1181.
- Teira, E., José Pazó, M., Serret, P., & Fernández, E. (2001). Dissolved organic carbon production by microbial populations in the Atlantic Ocean. *Limnology and Oceanography*, 46(6), 1370–1377. <https://doi.org/10.4319/lo.2001.46.6.1370>
- Thunell, R., Benitez-Nelson, C., Varela, R., Astor, Y., & Muller-Karger, F. (2007). Particulate organic carbon fluxes along upwelling-dominated continental margins: Rates and mechanisms. *Global Biogeochemical Cycles*, 21(1). <https://doi.org/10.1029/2006GB002793>
- Tortell, P. D., Asher, E. C., Ducklow, H. W., Goldman, J. A. L., Dacey, J. W. H., Grzymalski, J. J., et al. (2014). Metabolic balance of coastal Antarctic waters revealed by autonomous pCO<sub>2</sub> and Delta O<sub>2</sub>/Ar measurements. *Geophysical Research Letters*, 41(19), 6803–6810. <https://doi.org/10.1002/2014GL061266>
- Uitz, J., Stramski, D., Reynolds, R. A., & Dubranna, J. (2015). Assessing phytoplankton community composition from hyperspectral measurements of phytoplankton absorption coefficient and remote-sensing reflectance in open-ocean environments. *Remote Sensing of Environment*, 171, 58–74. <https://doi.org/10.1016/j.rse.2015.09.027>
- Wang, S., Kranz, S. A., Kelly, T. B., Song, H., Stukel, M. R., & Cassar, N. (2020). Lagrangian studies of net community production: The effect of diel and multi-day non-steady state factors and vertical fluxes on O<sub>2</sub>/Ar in a dynamic upwelling region. *Journal of Geophysical Research: Biogeosciences*, 125, e2019JG005569. <https://doi.org/10.1029/2019JG005569>
- Yool, A., Martin, A. P., Fernandez, C., & Clark, D. R. (2007). The significance of nitrification for oceanic new production. *Nature*, 447(7147), 999–1002. <https://doi.org/10.1038/nature05885>